Chapter 2

Comparison of Two BBN Codes

This author first had to determine if the Texas code's results were correct. So this author ran the code first with the nuclear reaction rates listed in TSOF. (TSOF was unclear on how they handled the reverse direction of their β-decay rates, and this author initially assumed that one just had to add the abundances of decaying isotopes to the abundances of the stable isotopes they decayed into to account for β-decay.) Also, the Texas code's values of constants such as the speed of light were updated to their most accurate measurements available. With these modification the Texas code first went from 30 rates to 119 and from 9 isotopes to 45.

Figures (2.1) showed the Texas code results before this author modified it in any way. The figures showed the mass fraction for ^{4}He and the ratios of isotope abundance to free proton abundance for the other isotopes, all as functions of η_{10}. Abundances of isotopes that decay, such as ^{7}Be and ^{11}C, were added into the abundances of the stable isotopes they decay into. But these results for ^{10}B and ^{11}B were smaller than the results reported in TSOF and in (Thomas, 1994) [14], by several orders of magnitude. Three reactions in

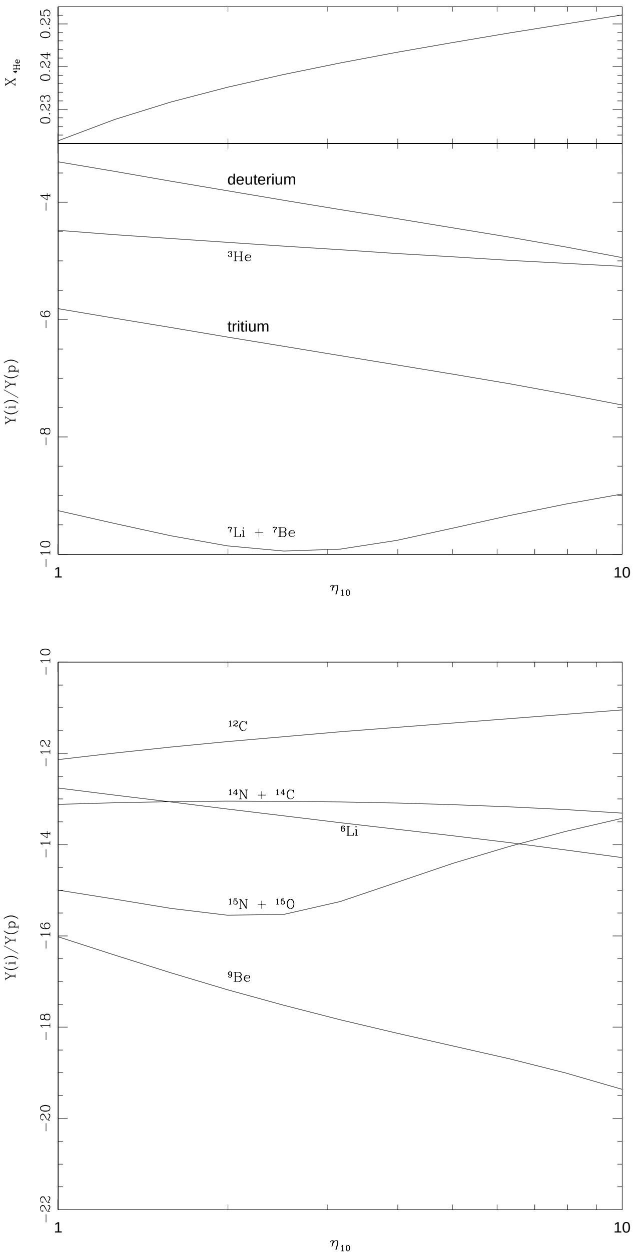

Figure 2.1: The Abundances (Mass fraction for ^{4}He produced by the Texas code before the revisions of this dissertation were implemented. Continued on next page.

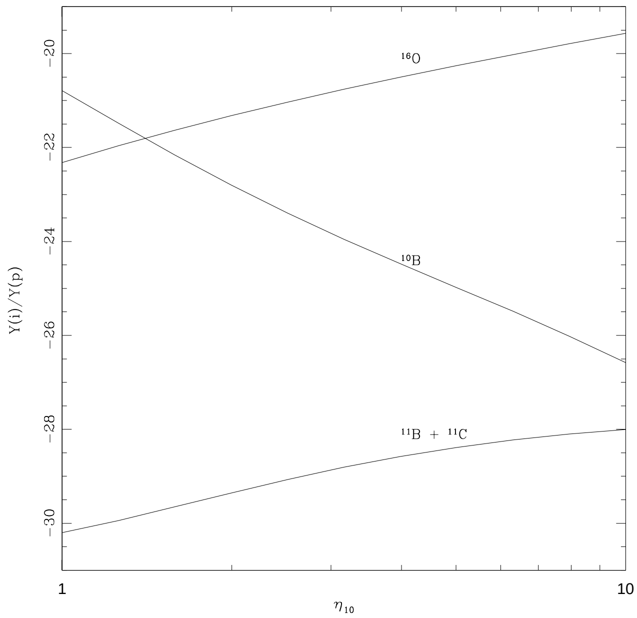

TSOF

$$
\begin{aligned}
{}^{10}\mathrm{B} + {}^{4}\,\mathrm{He} &\leftrightarrow {}^{14}\mathrm{N} + \gamma \\
{}^{11}\mathrm{B} + {}^{4}\,\mathrm{He} &\leftrightarrow {}^{15}\mathrm{N} + \gamma \\
{}^{11}\mathrm{C} + {}^{4}\,\mathrm{He} &\leftrightarrow {}^{15}\mathrm{O} + \gamma
\end{aligned}
$$

severely depleted ^{10}B, ^{11}B, and ^{11}C for all values of η_{10}. Figure (2.2a) showed $Y(i)/Y(\mathrm{p})$ for ^{10}B and ^{11}B + ^{11}C both with and without those three rates. The removal of the first reaction allowed ^{10}B to survive, reaching within the reported margin of error of (Thomas 1994)'s results. But for higher values of η_{10} the Texas code produced too much ^{11}B+^{11}C. This author started correspondence with David Thomas about the results in his articles, and worked in the reactions and isotopes listed in TSOMMF in addition to the reaction

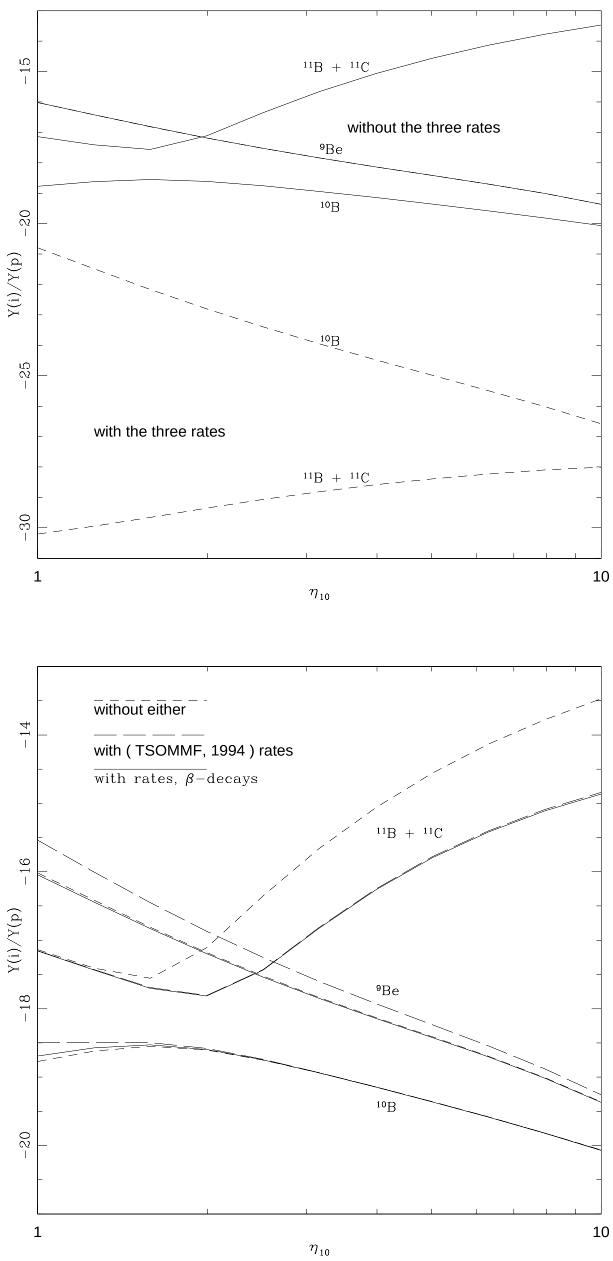

Figure 2.2: (2.2a) shows how the three reaction rates mentioned in the text severely deplete ^{9}Be, ^{10}B, and ^{11}B+^{11}C. (2.2b) shows how those isotope abundances change due to the nuclear rates in (TSOMMF, 1994) and the β-decays.

in TSOF. In 1995 Thomas e-mailed the Thomas et al code used for TSOF and TSOMMF. In writing the (Thomas 1994) article Thomas apparently had commented out of the Thomas et al code the three rates in question. The Thomas et al code also did not have reverse rates for any of the β-decays except for neutron decay. This author worked in the β-decay rates into the Texas code according to the Thomas et al code's model. Figure (2.2b) showed the results for ^{9}Be, ^{10}B and ^{11}B+^{11}C with just the new nuclear reactions from TSOMMF added, and then with those rates plus the β-decays added. These new rates reduced ^{11}B+^{11}C to within the range of (Thomas 1994).

None of the alterations discussed above affected the Texas code's value of $X_{^4\mathrm{He}}$ more than an order of 10^{-6}. But Figure (2.3) showed that at this point the codes disagreed on the value of $X_{^4\mathrm{He}}$ on the order of 0.003, regardless of the value of η_{10}. For $\eta_{10} = 3.0$ the Texas code gave an $X_{^4\mathrm{He}}$ greater by 0.0036 than the Thomas et al code gave (See Table (2.1)). That difference was more than order of magnitude greater than the change in $X_{^4\mathrm{He}}$ due to neutrino heating as reported in some articles ([30], [31], [32]). The scheme by which the Texas code went about solving for the isotope abundances and other physical quantities might've been erroneously conceive, or the sheme might've made the calculations using approximate methods now considered obsolete because of computer speed and accuracy.

The next section outlines detailed traces of how both the Texas code and the Thomas et al code evolve the standard model of the universe from an initial temperature T = 100 GK down to T = 0.01 GK. The traces have many differences, the significance of each difference this author determines. The section after discusses what changes to make in both codes to get $X_{^4He}$ in each of them to agree to within 0.0001.

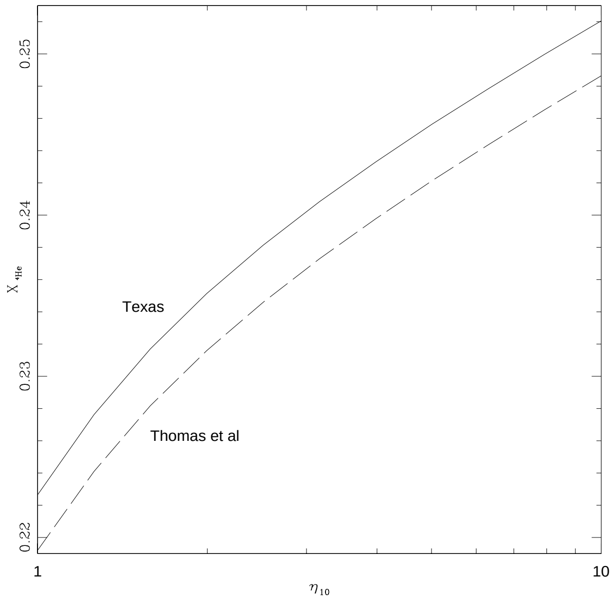

Figure 2.3: The Abundances (Mass fraction for ^{4}He produced by the Texas code before the revisions of this dissertation were implemented. (Continued on next page.)

2.1 Trace of Each Code

A trace describes the initial conditions each of the two codes start out with, and the calculations each code makes to advance by one timestep.

2.1.1 The Texas Code: Trace

The Texas code starts at a temperature $T = 100$ GK of the photons, electrons/positrons, and the neutrinos. In its standard model form, this code initiallizes the thermal quantities listed below according to equations listed in WFH [6].

isotope	Thomas et al X	Texas X
n	$0.7708255683 \times 10^{-15}$	$0.5911523509 \times 10^{-15}$
p	0.7631366158	0.7596024488
d	$0.1204559811 \times 10^{-3}$	$0.124011266 \times 10^{-3}$
^{3}H	$0.5796268916 \times 10^{-6}$	$0.5998407526 \times 10^{-6}$
^{3}He	$0.3616138099 \times 10^{-4}$	$0.3644216616 \times 10^{-4}$
^{4}He	0.2369001572	0.2402364976
^{6}Li	$0.1421012168 \times 10^{-12}$	$0.1490691574 \times 10^{-12}$
^{7}Li	$0.3351128337 \times 10^{-9}$	$0.3508710629 \times 10^{-9}$
^{7}Be	$0.2862168792 \times 10^{-9}$	$0.2675716413 \times 10^{-9}$
^{9}Be	$0.1038293451 \times 10^{-16}$	$0.1132389445 \times 10^{-16}$
^{10}B	$0.8947581823 \times 10^{-18}$	$0.9709129222 \times 10^{-18}$
^{11}B	$0.9518929095 \times 10^{-16}$	$0.9127661864 \times 10^{-16}$
^{12}C	$0.2887567361 \times 10^{-13}$	$0.3077248267 \times 10^{-13}$
^{13}C	$0.1974028406 \times 10^{-14}$	$0.2081962054 \times 10^{-14}$
^{14}C	$0.6206298819 \times 10^{-13}$	$0.6654359083 \times 10^{-13}$
^{14}N	$0.1271319722 \times 10^{-12}$	$0.1336873955 \times 10^{-12}$
^{16}O	$0.7261706627 \times 10^{-17}$	$0.7809972963 \times 10^{-17}$
^{19}F	$0.354880987 \times 10^{-21}$	$0.7635245978 \times 10^{-24}$
^{20}F	$0.562559098 \times 10^{-21}$	$0.3832735807 \times 10^{-24}$
^{21}Ne	$0.6863082969 \times 10^{-21}$	$0.5603940113 \times 10^{-23}$

Table 2.1: The mass fractions from each code before any modifications were made. ($\eta_{10} = 3$).

$$
\begin{aligned}
a &= \frac{\pi^2}{15}\frac{k^4}{(c\hbar)^3} \\
E &= \frac{m_e}{kT} \\
\rho_\gamma &= aT^4 \\
n_\gamma &= \frac{30(1.202)}{k\pi^4}aT^3 \\
\rho_{\mathrm{e}} &= \frac{30}{\pi^4}aT^4\int_0^\infty dX\,\frac{X^2\sqrt{X^2+E^2}}{e^{\sqrt{X^2+E^2}}+1} \\
P_{\mathrm{e}} &= \frac{10}{\pi^4}aT^4\int_0^\infty dX\,\frac{X^4}{\sqrt{X^2+E^2}(e^{\sqrt{X^2+E^2}}+1)}
\end{aligned}
$$

$$
\begin{aligned}
N_{\mathrm{e}} &= \frac{30}{k\pi^4} a T^3 \int_0^\infty dX \frac{X^2}{e^{\sqrt{X^2+E^2}}+1} \\
\rho_\nu &= \frac{7}{8} a T_\nu^4 && (2.1) \\
\rho_b R^3 &= \text{const} && (2.2) \\
\rho_b &= m_N n_\gamma \eta && (2.3)
\end{aligned}
$$

The code uses the assumption that $\rho_\nu R^4$ is constant to determine R. R can then be initiallized to $R = T_{\nu_o}/T$, where $T_{\nu_o} = 1.946$ K is the present-day neutrino temperature. The code also assumes that $\rho_b R^3$ stays constant for all time (R^3 is equivalent to volume V) and so uses the present-day ρ_{b_o}, calculated from η, to initiallize ρ_b. Abundances for neutrons and protons are set

$$
\begin{aligned}
Y(\mathrm{n}) &= \frac{1}{e^{\frac{m_{\mathrm{n}}-m_{\mathrm{p}}}{kT}}+1} \\
Y(\mathrm{p}) &= 1 - Y(\mathrm{n})
\end{aligned}
$$

based on the fact that neutrons and protons are in equilibrium with each other at the highest temperatures. All the other abundances are set to zero.

The Texas code starts a timestep n by calculating the reaction rates taken at the $\mathrm{e}^\pm + \gamma$ plasma temperature T and the neutrino temperature T_ν. For the nuclear reaction rates the code has algebraic formulii that depend on T and ρ_b. For the six weak reactions that interconvert neutrons and protons the Texas code numercially solves their integral equations.

$$
\begin{aligned}
\lambda(\mathrm{n} + \nu_e \to \mathrm{p} + \mathrm{e}^-) &= \frac{1}{\tau_{\mathrm{n}}\lambda_0} \int v_{\mathrm{e}} E_{\mathrm{e}}^2 p_{\nu_{\mathrm{e}}}^2 dp_{\nu_{\mathrm{e}}} f_{\nu_{\mathrm{e}}} (1 - f_{\mathrm{e}}) \\
\lambda(\mathrm{n} + \mathrm{e}^+ \to \mathrm{p} + \bar{\nu_{\mathrm{e}}}) &= \frac{1}{\tau_{\mathrm{n}}\lambda_0} \int p_{\nu_{\mathrm{e}}}^2 p_{\mathrm{e}}^2 dp_{\mathrm{e}} f_{\mathrm{e}} (1 - f_{\nu_{\mathrm{e}}})
\end{aligned}
$$

$$
\begin{aligned}
\lambda(\mathrm{n} \rightarrow \mathrm{p} + \mathrm{e}^- + \bar{\nu}_\mathrm{e}) &= \frac{1}{\tau_\mathrm{n}\lambda_0}\int v_\mathrm{e} p_{\nu_\mathrm{e}}^2 E_\mathrm{e}^2 dp_{\nu_\mathrm{e}}(1-f_{\nu_\mathrm{e}})(1-f_\mathrm{e}) \\
\lambda(\mathrm{p} + \mathrm{e}^- \rightarrow \mathrm{n} + \nu_\mathrm{e}) &= \frac{1}{\tau_\mathrm{n}\lambda_0}\int p_{\nu_\mathrm{e}}^2 p_\mathrm{e}^2 dp_\mathrm{e} f_\mathrm{e}(1-f_{\nu_\mathrm{e}}) \\
\lambda(\mathrm{p} + \bar{\nu}_\mathrm{e} \rightarrow \mathrm{n} + \mathrm{e}^+) &= \frac{1}{\tau_\mathrm{n}\lambda_0}\int v_\mathrm{e} E_\mathrm{e}^2 p_{\nu_\mathrm{e}}^2 dp_{\nu_\mathrm{e}} f_{\nu_\mathrm{e}}(1-f_\mathrm{e}) \\
\lambda(\mathrm{p} + \mathrm{e}^- + \bar{\nu}_\mathrm{e} \rightarrow \mathrm{n}) &= \frac{1}{\tau_\mathrm{n}\lambda_0}\int v_\mathrm{e} p_{\nu_\mathrm{e}}^2 E_\mathrm{e}^2 dp_{\nu_\mathrm{e}} f_{\nu_\mathrm{e}} f_\mathrm{e}
\end{aligned}
$$

f_e and f_{ν_e} are the distribution functions of electrons and electron neutrinos (and their corresponding antiparticles). In the standard model they have Fermi-Dirac distributions.

$$
\begin{aligned}
f_\mathrm{e}(E,T) &= \frac{1}{1+e^{\frac{E}{kT}}} \\
f_{\nu_\mathrm{e}}(E_\nu,T_\nu) &= \frac{1}{1+e^{\frac{E_\nu}{kT_\nu}}}
\end{aligned}
$$

These weak rates should be normalized so that the expression corresponding to neutron decay goes to $1/\tau_n$ as T, T_ν goes to 0. Therefore the code divides all the weak rates by λ_0.

$$
\lambda_0 = \int v_\mathrm{e} p_{\nu_\mathrm{e}}^2 E_\mathrm{e}^2 dp_{\nu_\mathrm{e}}
$$

The Texas code sets $\lambda_0 = 10/6$.

Theoretically the code can calculate the time derivative of $Y(i)$ using the equation from (Wagoner, 1969) [7]

$$
\frac{dY(i)}{dt} = \sum_{j,k,l} N_i \left(-\frac{Y^{N_i}(i)Y^{N_j}(j)}{N_i!N_j!}[ij] + \frac{Y^{N_k}(k)Y^{N_l}(l)}{N_k!N_l!}[kl] \right) \tag{2.4}
$$

which applies to a reaction of the form:

$$N_i\left({}^{A_i}Z_i\right) + N_j\left({}^{A_j}Z_j\right) \quad \leftrightarrow \quad N_k\left({}^{A_k}Z_k\right) + N_l\left({}^{A_l}Z_l\right)$$

($[ij]$ is the forward direction reaction rate, $[kl]$ is the reverse direction.) After calculating $dY(i)/dt$ the code should then calculate $Y(i)$ for the next timestep $(n+1)$ using a Runge-Kutta scheme

$$Y_{n+1}(i) \quad = \quad Y_n(i) + \frac{1}{2}\left[\frac{dY(i)}{dt}(t, Y_n) + \frac{dY(i)}{dt}(t+\Delta t, Y_{n+1})\right]\Delta t \qquad (2.5)$$

that should give values of $Y(i)$ that have second-order convergence for smaller values of timestep difference Δt. But as Peebles [5], WFH [6], and Wagoner [7] all pointed out Equation (2.4) involves the proportionaly small difference between two very large numbers for high temperatures T. The Texas code gets around solving for this difference by linearizing the right-hand side of Equation (2.4) in a manner similar to (Wagoner, 1969).

$$\begin{aligned}\frac{Y_{n\alpha}(i) - Y_n(i)}{\Delta t_n} \quad = \quad & \sum_{i,j,k} -\frac{N_i[ij]}{N_i!N_j!(N_i+N_j)} \\ & [N_i Y_n^{N_i-1}(i) Y_n^{N_j}(j) Y_{n\alpha}(i) + N_j Y_n^{N_i}(i) Y_n^{N_j-1}(j) Y_{n\alpha}(j)] \\ & + \frac{N_i[kl]}{N_k!N_l!(N_k+N_l)}[N_k Y_n^{N_k-1}(k) Y_n^{N_l}(l) Y_{n\alpha}(k) + \\ & N_l Y_n^{N_k}(k) Y_n^{N_l-1}(l) Y_{n\alpha}(l)] \end{aligned} \qquad (2.6)$$

A term such as $Y_n(i)Y_n(j)$ that is nonlinear in Y_n has been replaced by an averaging expression $1/2(Y_{n\alpha}(i)Y_n(j) + Y_n(i)Y_{n\alpha}(j))$ that is linear in $Y_{n\alpha}$. The following section on the abundances' convergence discusses what $Y_{n\alpha}$ could mean specifically. The values of $Y_{n\alpha}$ are unknown. But one can rearrange Equation (2.6) into a matrix equation for $Y_{n\alpha}$.:

$$Y_n(i) \quad = \quad Q_{ij}\left(Y_n, [ij](T_n), [kl](T_n)\right) \times Y_{n\alpha}(j) \tag{2.7}$$

The matrix elements Q_{ij} consist of terms that depend on $Y_n(i)$, the abundances taken at time t_n and temperature T_n, and forward and reverse reaction rates $[ij]$ and $[kl]$, which also are taken at T_n. The Texas code solves for $Y_{n\alpha}$, and then plugs $Y_{n\alpha}$ back into the left-hand side of Equation (2.6) to get an expression for $dY(i)/dt$ taken at time t_n.

$$\frac{dY(i)}{dt}(t, Y_n) \quad \doteq \quad \frac{Y_{n\alpha}(i) - Y_n(i)}{\Delta t_n} \tag{2.8}$$

Note that in Equation (2.7) the Texas code uses Y_n in both the left-hand side and the matrix on the right-hand side, and the timestep difference $\Delta t_n = t_{n+1} - t_n$.

The Texas code also evolves $\ln R$ and $\rho_{\mathrm{e}+\gamma}$ using the second order Runge-Kutta method. Assuming a Friedmann-Robertson-Walker model of the universe and the universe as a perfect fluid:

$$\begin{aligned} ds^2 &= dt^2 - R^2(t)\frac{dr^2 + r^2\left(d\theta^2 + \sin^2\theta d\phi^2\right)}{\left(1 + \frac{1}{4}kr^2\right)^2} \\ T^{ab} &= (\rho + p)U^a U^b - pg^{ab} \end{aligned}$$

One can derive equations for $\dot{R}$ and $\dot{\rho}_{\mathrm{e}+\gamma}$ from the Einstein field equations and the energy conservation law $T^{0b}{}_{;b}$, where T^{ab} is the stress-energy tensor.

$$\frac{\dot{R}}{R} \quad = \quad \sqrt{\frac{8}{3}\pi G(\rho_\gamma + \rho_{\mathrm{e}} + \rho_\nu)} \tag{2.9}$$

$$
\begin{aligned}
\dot{\rho}_{\mathrm{e}+\gamma} &= -3\frac{\dot{R}}{R}(p_{\mathrm{e}+\gamma} + \rho_{\mathrm{e}+\gamma}) \\
\dot{\rho}_{\mathrm{e}+\gamma} &= -4\frac{\dot{R}}{R}\rho_\gamma - 3\frac{\dot{R}}{R}(p_{\mathrm{e}} + \rho_{\mathrm{e}}) \qquad (2.10)
\end{aligned}
$$

(Pressure $p_\gamma = \rho_\gamma/3$ for massless photons.) With time derivatives for Y_i, $\ln R$ and $\rho_{e+\gamma}$ calculated, the code can evolve these quantities to new interim values, indicated by a $\tilde{}$ symbol.

$$
\begin{aligned}
\tilde{Y}_n(i) &= Y_n(i) + \frac{dY(i)}{dt}(t, Y_n(i))\Delta t_n \qquad (2.11) \\
(\tilde{\ln R})_n &= (\ln R)_n + \left[\frac{\dot{R}}{R}(t, \rho(T_n))\right]\Delta t_n \\
(\tilde{\rho}_{\mathrm{e}+\gamma})_n &= (\rho_{\mathrm{e}+\gamma})_n + \left[\dot{\rho}_{\mathrm{e}+\gamma}(t, \rho(T_n), p(T_n))\right]\Delta t_n
\end{aligned}
$$

The code has to derive a new electromagnetic plasma temperature $\tilde{T}_n$ from $\tilde{\rho}_{\mathrm{e}+\gamma}$. To do that the code can make an interpolation table of values of T and $\rho_{\mathrm{e}+\gamma}$ at the start of the run, and then interpolate a $\tilde{T}_n$ if $\tilde{T}_n$ is within the range of [0.5, 11] GK. For $T > 11$ GK the code approximates $\rho_e = (7/4)aT^4$ (massless electrons), and the code can set $\rho_e = 0$ for $T < 0.5$ GK. This author has also added an option of instead using Newton's method to determine $\tilde{T}_n$, where the code defines a function

$$
F_{Newt}(T) = (\rho_\gamma(T) + \rho_{\mathrm{e}}(T)) - \tilde{\rho}_{\mathrm{e}+\gamma}
$$

and find a $\tilde{T}_n$ where $F(\tilde{T}_n)$ is closest to 0.0. Using Newton's method the code can calculate $\tilde{T}_n$ down to $10^{-6}\tilde{T}_n$. The data in Table (2.1) is calculated using the Newton's method. Table (2.2) compares that data with the Texas code's data using the interpolation table instead. The table increases $X_{^4\mathrm{He}}$ by 0.0002.

isotope	Table	Newton
n	$0.5796672533 \times 10^{-15}$	$0.5911523509 \times 10^{-15}$
p	0.7593842304	0.7596024488
d	$0.1227367267 \times 10^{-3}$	$0.124011266 \times 10^{-3}$
^{3}H	$0.5937885224 \times 10^{-6}$	$0.5998407526 \times 10^{-6}$
^{3}He	$0.3627340187 \times 10^{-4}$	$0.3644216616 \times 10^{-4}$
^{4}He	0.2404561653	0.2402364976
^{6}Li	$0.147755779 \times 10^{-12}$	$0.1490691574 \times 10^{-12}$
^{7}Li	$0.3480477024 \times 10^{-9}$	$0.3508710629 \times 10^{-9}$
^{7}Be	$0.273632891 \times 10^{-9}$	$0.2675716413 \times 10^{-9}$
^{9}Be	$0.1111350145 \times 10^{-16}$	$0.1132389445 \times 10^{-16}$
^{10}B	$0.9599813074 \times 10^{-18}$	$0.9709129222 \times 10^{-18}$
^{11}B	$0.9642233745 \times 10^{-16}$	$0.9127661864 \times 10^{-16}$
^{12}C	$0.3122213502 \times 10^{-13}$	$0.3077248267 \times 10^{-13}$
^{13}C	$0.2135721042 \times 10^{-14}$	$0.2081962054 \times 10^{-14}$
^{14}C	$0.6705199821 \times 10^{-13}$	$0.6654359083 \times 10^{-13}$
^{14}N	$0.1347814796 \times 10^{-12}$	$0.1336873955 \times 10^{-12}$
^{16}O	$0.7945787317 \times 10^{-17}$	$0.7809972963 \times 10^{-17}$
^{19}F	$0.7714050623 \times 10^{-24}$	$0.7635245978 \times 10^{-24}$
^{20}F	$0.3687825758 \times 10^{-24}$	$0.3832735807 \times 10^{-24}$
^{21}Ne	$0.5691361335 \times 10^{-23}$	$0.5603940113 \times 10^{-23}$

Table 2.2: The Texas Code's mass fractions when run using the Interpolation Table and when run using Newton's Method to account the evolution of $\rho_{\mathrm{e}+\gamma}$ during the epoch of $\mathrm{e}^-\mathrm{e}^+$ annihilation.

Once $\tilde{T}_n$ is known the Texas code can then calculate $(\tilde{p}_e)_n$ and $(\tilde{n}_e)_n$. The code uses Equations (2.1) and (2.2) to calculate ρ_b and ρ_ν.

The code then calculates the second R-K time derivatives of $\ln R$ and $\rho_{\mathrm{e}+\gamma}$, and then the final values $(\ln R)_{n+1}$ and $(\rho_{\mathrm{e}+\gamma})_{n+1}$.

$$
\begin{aligned}
(\ln R)_{n+1} &= (\ln R)_n + \frac{1}{2}\left[\frac{\dot{R}}{R}(t, \rho(T_n)) + \frac{\dot{R}}{R}(t + \Delta t_n, \rho(\tilde{T}_n))\right]\Delta t_n \\
(\rho_{\mathrm{e}+\gamma})_{n+1} &= (\rho_{\mathrm{e}+\gamma})_n \\
&\quad + \frac{1}{2}\left[\dot{\rho}_{\mathrm{e}+\gamma}(t, \rho(T_n), p(T_n)) + \dot{\rho}_{\mathrm{e}+\gamma}(t + \Delta t_n, \rho(\tilde{T}_n), p(\tilde{T}_n))\right]\Delta t_n
\end{aligned}
$$

From $(\rho_{e+\gamma})_{n+1}$ the Texas code gets T_{n+1}. It uses T_{n+1} to calculate new values for the reaction rates $[ij]$ and $[kl]$. The code's equation for the second R-K derivative of $Y(i)$ is:

$$\begin{aligned}
\frac{Y_{n\beta}(i) - Y_n(i)}{\Delta t_n} &= \sum_{i,j,k} -\frac{N_i[ij]}{N_i!N_j!(N_i+N_j)} \\
&\quad [N_i \tilde{Y}_n^{N_i-1}(i)\tilde{Y}_n^{N_j}(j)Y_{n\beta}(i) + N_j \tilde{Y}_n^{N_i}(i)\tilde{Y}_n^{N_j-1}(j)Y_{n\beta}(j)] \\
&\quad + \frac{N_i[kl]}{N_k!N_l!(N_k+N_l)}[N_k \tilde{Y}_n^{N_k-1}(k)\tilde{Y}_n^{N_l}(l)Y_{n\beta}(k) + \\
&\quad N_l \tilde{Y}_n^{N_k}(k)\tilde{Y}_n^{N_l-1}(l)Y_{n\beta}(l)] \qquad (2.12) \\
Y_n(i) &= Q_{ij}\left(\tilde{Y}_n, [ij](T_{n+1}), [kl](T_{n+1})\right) \times Y_{n\beta}(j) \qquad (2.13)
\end{aligned}$$

Here Equation (2.4) is written in a form linear in $Y_{n\beta}$, a new set of unknown abundances that the Texas code solves for. The new matrix elements Q_{ij} that the code constructs use the interim values $\tilde{Y}_n$, but the final values of $[ij]$ and $[kl]$. The code defines as its second R-K derivative:

$$\begin{aligned}
\frac{dY(i)}{dt}(t+\Delta t_n, \tilde{Y}_n) &\doteq \frac{Y_{n\beta}(i) - Y_n(i)}{\Delta t} \\
Y_{n+1}(i) &= Y_n(i) + \frac{1}{2}\left[\frac{dY(i)}{dt}(t, Y_n) + \frac{dY(i)}{dt}(t+\Delta t_n, \tilde{Y}_n)\right]\Delta t_n
\end{aligned}$$

With all quantities determined for time t_{n+1} the Texas code calculates the next timestep difference Δt_{n+1}:

$$\Delta t_{n+1} = dk \min\left[\frac{Y_{n+1}(i)}{\frac{dY(i)}{dt}}, \frac{(\ln R)_{n+1}}{\frac{\dot{R}}{R}}, \frac{(\rho_{e+\gamma})_{n+1}}{\dot{\rho}_{e+\gamma}}\right] \qquad (2.14)$$

The time derivatives in Equation (2.14) are the averages of the two R-K derivatives. The Texas code follows this process for all timesteps until T falls below 0.01 GK.

2.1.2 The Thomas et al Code: Trace

The Thomas et al code initializes $Y(\mathrm{n})$ and $Y(\mathrm{p})$ the same was as the Texas code does. But it sets all the other abundances to a non-zero minimum $Y_{\mathrm{min}} = 10^{-25}$, except for the deuterium abundance $Y(\mathrm{d})$ which has an abundance larger than Y_{min} from $T = 100$ GK on. The Thomas et al code initialize $Y(d)$ with the equation for Nuclear Statistical Equilibrium (NSE).

$$
\begin{aligned}
X_i &= \frac{g_i}{2}\left(2(1.202)\sqrt{\frac{2}{\pi}}\right)^{A_i-1} A_i^{5/2}\left(\frac{kT}{m_N}\right)^{3(A_i-1)/2} \eta^{A_i-1} X_p^{Z_i} X_n^{A_i-Z_i} e^{\frac{B}{kT}} \\
B &= Z_i m_p + (A_i - Z_i) m_n - m_i
\end{aligned}
$$

One can derive this equation by using the Maxwell-Boltzmann distribution as a good approximation of the distribution functions of the highly nonrelativistic nuclei. The Texas code assumes that the electron chemical potential $\phi_{\mathrm{e}} = 0.0$, and therefore $n_{\mathrm{e}^-} = n_{\mathrm{e}^+}$. The Thomas et al code accounts for a nonzero ϕ_{e}, taking ϕ_{e} at $T = 100$ GK as input instead of the Texas code's ρ_b at $T =$ the current 2.726 K. The Thomas et al code uses ϕ_{e} in an equation for the difference $n_{\mathrm{e}^-} - n_{\mathrm{e}^+}$ derived from the Bessel expansions of the integral equations for $n_{\mathrm{e}^\pm}$ [33]:

$$
n_{\mathrm{e}^-} - n_{\mathrm{e}^+} = \frac{2}{15}\frac{m_{\mathrm{e}}^3}{k^4}\sum_{n=1}^{\infty}\sinh(n\phi_{\mathrm{e}})L(nz)
$$

where $z = m_{\mathrm{e}}/kT$ and the $L(nz)$ are Bessel functions. Charge conservation requires that this difference equal the proton number density.

$$
n_{\mathrm{e}^-} - n_{\mathrm{e}^+} = \frac{\rho_b S}{m_N} \tag{2.15}
$$

$S = \sum_i Z_i Y(i)$. The code defines a variable h_v such that

$$\rho_b \;=\; h_v a \frac{15}{\pi^2} T^3$$

So $\phi_{\rm e}$ determines $n_{\rm e^-} - n_{\rm e^+}$, which determines ρ_b and that determines η_{10}. The quantities ρ_γ, $\rho_{\rm e}$, $p_{\rm e}$ and ρ_ν are initialized using the same equations as the Texas code.

Instead of evolving $\rho_{\rm e+\gamma}$ and $\ln R$, the Thomas et al code evolves T, h_v, and $\phi_{\rm e}$. To derive the equation for dT/dt the code starts with the energy conservation equation.

$$\begin{aligned}
\frac{d\rho_{\rm e+\gamma}}{dT}\frac{dT}{dt} &= -3\frac{\dot R}{R}(p_{\rm e+\gamma} + \rho_{\rm e+\gamma}) \\
\frac{dT}{dt} &= -\frac{3\frac{\dot R}{R}(p_{\rm e+\gamma} + \rho_{\rm e+\gamma})}{\frac{d\rho_\gamma}{dT} + \frac{d\rho_{\rm e}}{dT}}
\end{aligned} \tag{2.16}$$

But in calculating $d\rho_{\rm e}/dT$ the code also takes into account the time dependence of $\phi_{\rm e}$.

$$\begin{aligned}
\frac{d\rho_{\rm e}}{dT} &= \frac{\partial \rho_{\rm e}}{\partial T} + \frac{\partial \rho_{\rm e}}{\partial \phi_{\rm e}}\frac{\partial \phi_{\rm e}}{\partial T} \\
\frac{\partial \rho_{\rm e}}{\partial \phi_{\rm e}} &= \frac{2}{15} a (zT)^4 \sum_{n=1}^{\infty} \frac{(-1)^{n+1}}{z} \sinh(n\phi_{\rm e}) M(nz)
\end{aligned}$$

The code uses a Bessel expansion of $\rho_{\rm e^-} + \rho_{\rm e^+}$ to get the expression for $\partial\rho_{\rm e}/\partial\phi_{\rm e}$. One gets the expression for $\partial\phi_{\rm e}/\partial T$ by dividing Equation (2.15) by T^3. Defining $N(T, \phi_e)$ as the left-hand side of (2.15) and $M(T, S, R)$ as the right-hand side:

$$
\begin{aligned}
M(T,S,R) &= \frac{\rho_b S}{m_N T^3} \\
N(T,\phi_e) &= \frac{2}{15}\frac{az^3}{k}\sum_{n=1}^{\infty}(-1)^{n+1}\sinh(n\phi_{\mathrm{e}})L(nz) \\
\frac{\partial\phi_{\mathrm{e}}}{\partial T} &= \frac{\frac{\partial M}{\partial T}-\frac{\partial N}{\partial T}}{\frac{\partial N}{\partial\phi_{\mathrm{e}}}}
\end{aligned}
$$

dh_v/dt is easily derived from the equation $h_v = \mathrm{const}/(RT)^3$.

$$
\frac{dh_v}{dt} = -3h_v\left(\frac{1}{R}\frac{dR}{dt}+\frac{1}{T}\frac{dT}{dt}\right) \tag{2.17}
$$

And from (2.15) one can derive equations for partial derivatives of ϕ_e with respect to R, S, and T.

$$
\begin{aligned}
\frac{d\phi_{\mathrm{e}}}{dt} &= \frac{\partial\phi_{\mathrm{e}}}{\partial T}\frac{dT}{dt}+\frac{\partial\phi_{\mathrm{e}}}{\partial R}\frac{dR}{dt}+\frac{\partial\phi_{\mathrm{e}}}{\partial S}\frac{dS}{dt} \\
\frac{d\phi_{\mathrm{e}}}{dt} &= \frac{\partial\phi_{\mathrm{e}}}{\partial T}\frac{dT}{dt}+\frac{\frac{3h_vS}{m_N}\frac{\dot{R}}{R}+\frac{h_v}{m_N}\sum_i Z_i\frac{dY(i)}{dt}}{\frac{\partial N}{\partial\phi_{\mathrm{e}}}}
\end{aligned} \tag{2.18}
$$

As with the Texas code the Thomas et al code starts a timestep t_n by calculating the nuclear reaction rates and the neutron/proton conversion rates. But the code's conversion rates also include radiative corrections discussed in detail in a 1982 PRD article by Dicus, et al (DKGSTT, 1982) [34]. Four of the weak reactions have a proton and electron on the same side. So the proton and electron could exchange a photon. (DKGSTT, 1982) showed that the correction to account for this photon exchange, the Coulomb correction, leads to an expression known as the Fermi factor.

$$
F(\beta) = \frac{\frac{2\pi\alpha}{\beta}}{1-e^{-\frac{2\pi\alpha}{\beta}}}
$$

β is the electron velocity v_e/c while α here is the fine structure constant. The Thomas et al code multiplies the integrands of these four reactions, and also of λ_0, with the Fermi factor. Other radiative corrections include self-energy photons emitted and absorbed by charged particles, and bremsstrahlung radiation. For these corrections, collectively known as the zero temperature radiative correction, (DKGSTT, 1982) derives another factor.

$$1 + \tfrac{\alpha}{2\pi} C(\beta, y)$$

$$\begin{aligned} C(\beta, y) &= 40 + 4(R_a - 1)\left[\frac{y}{3\epsilon} - \frac{3}{2} + \ln(2y)\right] + R_a \left[2(1+\beta^2) + \frac{y^2}{6\epsilon^2}\right. \\ &\quad \left. -4\beta R_a\right] - \frac{4}{(1+\beta)^6}[2 + 11\beta + 25\beta^2 + 30\beta^3 + 20\beta^4 + 8\beta^5] \end{aligned}$$

$\epsilon = E_e/m_e$ and $y = E_\nu/m_e$. The rapidity $R_a = (\text{arctanh}\beta)/\beta$. The integrands in all six of the rates and λ_0 are supposed to be multiplied by this factor. But instead of using the full blown expression the Thomas et al code rounds off this factor to a constant and works it into λ_0. The Thomas et al code has a λ_0 set to 1.691715. The Texas code therefore needs to have this new value of λ_0 and the Fermi factor worked into it.

At the start of a timestep t_n, the Thomas et al code has **not** calculated a value for Δt_n. In its equation for the first Runge-Kutta time derivative of $Y(i)$

$$\begin{aligned} \frac{Y_{n\alpha}(i) - Y_{n-1}(i)}{\Delta t_{n-1}} &= \sum_{i,j,k} -\frac{N_i[ij]}{N_i!N_j!(N_i+N_j)} \\ &\quad [N_i Y_n^{N_i-1}(i) Y_n^{N_j}(j) Y_{n\alpha}(i) + N_j Y_n^{N_i}(i) Y_n^{N_j-1}(j) Y_{n\alpha}(j)] \end{aligned}$$

$$
\begin{aligned}
& + \frac{N_i[kl]}{N_k!N_l!(N_k+N_l)}[N_k Y_n^{N_k-1}(k) Y_n^{N_l}(l) Y_{n\alpha}(k) + \\
& N_l Y_n^{N_k}(k) Y_n^{N_l-1}(l) Y_{n\alpha}(l)] \qquad (2.19)
\end{aligned}
$$

$$
Y_{n-1}(i) = Q_{ij}\left(Y_n, [ij](T_n), [kl](T_n)\right) \times Y_{n\alpha}(j) \qquad (2.20)
$$

it uses Δt_{n-1} instead of Δt_n in the denominator on the left-hand side. The code also uses Y_{n-1} on that side instead of Y_n, but the right-hand side is the same as in the Texas code. The following section on convergence will explain the significance of these differences between the codes. The Thomas et al code solves for $Y_{n\alpha}$ but defines

$$
\frac{dY(i)}{dt}(t, Y_n(i)) \doteq \frac{Y_{n\alpha}(i) - Y_{n-1}(i)}{\Delta t_{n-1}}
$$

At the point right after calculating $dY(i)/dt$ and dT/dt the Thomas et al code uses them to get a value for Δt_n.

$$
\begin{aligned}
\Delta t_n &= dk \min\left[\frac{Y_n(i)}{\dot{Y}_n(i)} dk_{\text{fac}}, \frac{T_n}{\frac{dT}{dt}}\right] \qquad (2.21) \\
dk_{\text{fac}} &= \left(1 + \left(-\frac{\log Y_n(i)}{dt_{\text{fac}}}\right)^2\right) \\
dt_{\text{fac}} &= -\frac{\log Y_{\min}}{\frac{dk_{\max}}{dk} - 1}
\end{aligned}
$$

The ratio $Y(i)/\dot{Y}(i)$ has this extra factor dk_{fac} that makes the code less likely to pick a value of Δt set by a $Y(i)$ close to $Y_{\min}$. An upcoming section on $Y_{\min}$ will discuss dk_{fac} in more detail. The Thomas et al code then uses Δt_n in updating $Y(i)$ and the three thermal quantities to their interim values.

$$
\tilde{Y}_n(i) = Y_n(i) + \frac{dY(i)}{dt}(t, Y_n(i)) \Delta t_n \qquad (2.22)
$$

$$\begin{aligned}
\tilde{T}_n &= T_n + \left[\frac{dT}{dt}(t, \rho(T_n))\right]\Delta t_n \\
(\tilde{h}_v)_n &= (h_v)_n + \left[\frac{dh_v}{dt}(t, R(T_n))\right]\Delta t_n \\
(\tilde{\phi}_e)_n &= (\phi_e)_n + \left[\frac{d\phi_d}{dt}(t, T_n, R(T_n), S(T_n))\right]\Delta t_n
\end{aligned}$$

With these new values, $\tilde{T}_n$ in particular, the code can calculate interim values for $[ij]$, $[kl]$, ρ_γ, ρ_{e}, p_{e}, ρ_b, and T_ν and ρ_ν. To determine T_ν the code uses the equation for the total entropy per unit volume, s.

$$\begin{aligned}
s &= \frac{R^3}{T}(\rho_{\gamma+\mathrm{e}^\pm} + p_{\gamma+\mathrm{e}^\pm}) \\
s &= \frac{4}{3}a(RT)^3 I\left(\frac{m_{\mathrm{e}}}{kT}\right) \qquad (2.23) \\
I(x) &= 1 + \frac{45}{2\pi^4}\int_0^\infty dy \frac{y}{e^{\sqrt{x^2+y^2}}+1}\left(\sqrt{x^2+y^2} + \frac{y^2}{3\sqrt{x^2+y^2}}\right)
\end{aligned}$$

The Thomas et al code calculates $I(m_{\mathrm{e}}/kT)$ for T and $T_o = 100$ GK. One can then use $RT_\nu =$ a constant and entropy conservation to get

$$\frac{T_o}{(T_\nu)_o}T_\nu = \left[\frac{I(x)}{I(x_o)}\right]^{\frac{1}{3}} T \qquad (2.24)$$

and $(T_\nu)_o = T_o$ at 100 GK. (The Texas code never needs to calculate the entropy.) Now the code calculates the second R-K derivative for $Y(i)$:

$$\begin{aligned}
\frac{Y_{n\beta}(i) - Y_n(i)}{\Delta t_n} = & \sum_{i,j,k} -\frac{N_i[ij]}{N_i!N_j!(N_i+N_j)} \\
& [N_i\tilde{Y}_n^{N_i-1}(i)\tilde{Y}_n^{N_j}(j)Y_{n\beta}(i) + N_j\tilde{Y}_n^{N_i}(i)\tilde{Y}_n^{N_j-1}(j)Y_{n\beta}(j)] \\
& + \frac{N_i[kl]}{N_k!N_l!(N_k+N_l)}[N_k\tilde{Y}_n^{N_k-1}(k)\tilde{Y}_n^{N_l}(l)Y_{n\beta}(k) + \\
& N_l\tilde{Y}_n^{N_k}(k)\tilde{Y}_n^{N_l-1}(l)Y_{n\beta}(l)] \qquad (2.25)
\end{aligned}$$

$$\begin{aligned} Y_n(i) &= Q_{ij}\left(\tilde{Y}_n, [ij](\tilde{T}_n), [kl](\tilde{T}_n)\right) \times Y_{n\beta}(j) \quad (2.26) \\ \frac{dY(i)}{dt}(t+\Delta t_n, Y_{n+1}(i)) &\doteq \frac{Y_{n\beta}(i) - Y_n(i)}{\Delta t_n} \end{aligned}$$

and for T, h_v and ϕ_e as well. Equation (2.26) is the same as Equation (2.13) in the Texas code, but the reaction rates are calculated at $\tilde{T}_n$ instead of T_{n+1}. The final values of the evolved variables are:

$$\begin{aligned} Y_{n+1}(i) &= Y_n(i) + \frac{1}{2}\left[\frac{dY(i)}{dt}(t, Y_n) + \frac{dY(i)}{dt}(t+\Delta t_n, Y_{n+1})\right]\Delta t_n \quad (2.27) \\ T_{n+1} &= T_n + \frac{1}{2}\left[\frac{dT}{dt}(t, \rho_n) + \frac{dT}{dt}(t+\Delta t_n, \rho(\tilde{T}_n))\right]\Delta t_n \\ (h_v)_{n+1} &= (h_v)_n + \frac{1}{2}\left[\frac{dh_v}{dt}(t, R_n) + \frac{dh_v}{dt}(t+\Delta t_n, R(\tilde{T}_n))\right]\Delta t_n \\ (\phi_e)_{n+1} &= (\phi_e)_n \\ &\quad + \frac{1}{2}\left[\frac{d\phi_e}{dt}(t, T_n, R_n, S_n) + \frac{d\phi_e}{dt}(t+\Delta t_n, \tilde{T}_n, R(\tilde{T}_n), S(\tilde{T}_n))\right]\Delta t_n \end{aligned}$$

This author adds in the zero-temperature radiative and Coulomb corrections into the Texas code. The correction to λ_0 decreases all of the neutron-proton converion rates. The rates convert fewer neutrons into protons, leaving more free neutrons around at the time of nucleosynthesis. $X_{^4He}$ increases due to this correction. But for the possible range of $\beta = [\ 0,\ 1\ ]$ the Fermi factor is always > 1. The Fermi factor increases the integrands of the four conversion rates where it applies. Since those integrands are always positive the Fermi factor increases those rates. These rates include neutron decay, which remains significant beyond all the other conversion rates. The Fermi factor has the opposite effect of increasing the conversion of neutrons to protons, leaving fewer

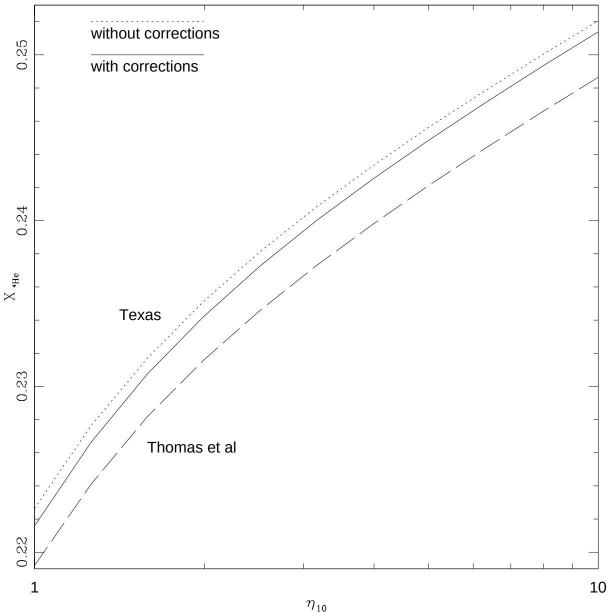

Figure 2.4: The zero-temperature radiative and the Coulomb corrections have the overall effect of decreasing $X_{^4\mathrm{He}}$ in the Texas code.

free neutrons to form ^{4}He at nucleosynthesis. It turns out that the Coulomb correction prevails over the correction to λ_0. Table (2.3) shows a decrease of $X_{^4He}$ by 0.0008, and Figure (2.4) shows that this decrease is independent of the value of η_{10}.

In Table (2.3), the codes have been rewritten with the most updated nuclear reaction equations, the values of the constants in agreement with each other, and with the conversion reactions including the radiative corrections. So the disagreements between the codes over physical quantities have been removed. At this point, the Texas code has a final $X_{^4\mathrm{He}} = 0.2393922575$ while the Thomas et al code has $X_{^4\mathrm{He}} = 0.2367002863$. The codes still have a disagreement of 0.0027. The next two sections look at the codes' different

iso.	Original	Corrections	Thomas et al
n	$0.5911523509 \times 10^{-15}$	$0.5891059898 \times 10^{-15}$	$0.7708255683 \times 10^{-15}$
p	0.7596024488	0.7604468206	0.7631366158
d	$0.124011266 \times 10^{-3}$	$0.1238741312 \times 10^{-3}$	$0.1204559811 \times 10^{-3}$
^{3}H	$0.5998407526 \times 10^{-6}$	$0.5991682496 \times 10^{-6}$	$0.5796268916 \times 10^{-6}$
^{3}He	$0.3644216616 \times 10^{-4}$	$0.3644816363 \times 10^{-4}$	$0.3616138099 \times 10^{-4}$
^{4}He	0.2402364976	0.2393922575	0.2367002863
^{6}Li	$0.1490691574 \times 10^{-12}$	$0.1482232092 \times 10^{-12}$	$0.1421012168 \times 10^{-12}$
^{7}Li	$0.3508710629 \times 10^{-9}$	$0.3489483673 \times 10^{-9}$	$0.3351128337 \times 10^{-9}$
^{7}Be	$0.2675716413 \times 10^{-9}$	$0.2680024313 \times 10^{-9}$	$0.2862168792 \times 10^{-9}$
^{9}Be	$0.1132389445 \times 10^{-16}$	$0.1123462846 \times 10^{-16}$	$0.1038293451 \times 10^{-16}$
^{10}B	$0.9709129222 \times 10^{-18}$	$0.9606638707 \times 10^{-18}$	$0.8927007279 \times 10^{-18}$
^{11}B	$0.9127661864 \times 10^{-16}$	$0.9145344794 \times 10^{-16}$	$0.9518929095 \times 10^{-16}$
^{12}C	$0.3077248267 \times 10^{-13}$	$0.3031417116 \times 10^{-13}$	$0.2887567361 \times 10^{-13}$
^{13}C	$0.2081962054 \times 10^{-14}$	$0.2052912964 \times 10^{-14}$	$0.1974028406 \times 10^{-14}$
^{14}C	$0.6654359083 \times 10^{-13}$	$0.6549885554 \times 10^{-13}$	$0.6206298819 \times 10^{-13}$
^{14}N	$0.1336873955 \times 10^{-12}$	$0.1319987799 \times 10^{-12}$	$0.1271319722 \times 10^{-12}$
^{16}O	$0.7809972963 \times 10^{-17}$	$0.7684340338 \times 10^{-17}$	$0.7261706627 \times 10^{-17}$
^{19}F	$0.7635245978 \times 10^{-24}$	$0.7499694297 \times 10^{-24}$	$0.354880987 \times 10^{-21}$
^{20}F	$0.3832735807 \times 10^{-24}$	$0.3717733241 \times 10^{-24}$	$0.562559098 \times 10^{-21}$
^{21}Ne	$0.5603940113 \times 10^{-23}$	$0.5466200682 \times 10^{-23}$	$0.6863082969 \times 10^{-21}$

Table 2.3: The Texas Code's mass fractions with the zero-temperature radiative correction and the Coulomb correction added into it, compared with the code's previous mass fractions and the mass fractions of the Thomas et al code

means of evolving $Y(i)$ for an explanation of the discrepency.

2.2 Convergence of the Codes

This section tests the convergence of $X_{^4\mathrm{He}}$ for each code. During a run, the magnitude of the timestep difference can vary from 10^{-8} to 10^{6}. Each code saves its timestep differences into a file. This author then runs each code reading the timestep differences from the file. Then each code runs with the differences halved, then quartered, and so forth, getting values of $X_{^4\mathrm{He}}$ for each number of divisions. Straight line fits for the data and the values to which the mass fractions eventually converge are determined using linear regression.

Define d as one over the number of divisions of the intial timestep difference (1/1, 1/2, 1/4, down to 1/128). $X_{^4\mathrm{He}}$ for the Thomas et al code best obeys the equation.

$$X_{^4\mathrm{He}} = 0.23905913 - (0.2472701063 \times 10^{-2})d^2$$

The equation has second-order convergence, as expected for the second order Runge-Kutta method. But $X_{^4\mathrm{He}}$ for the Texas code turns out to obey

$$X_{^4\mathrm{He}} = 0.2391420344 + (0.3830766191 \times 10^{-3})d$$

an equation first-order in d. These equations are illustrated in Figure (2.5). Something in the means of calculating $Y(i)$ is correct in the Thomas et al code but not in the Texas code.

Go back to Equation (2.5)

$$Y_{n+1}(i) = Y_n(i) + \frac{1}{2}\left[\left(\frac{dY(i)}{dt}\right)_n + \left(\frac{dY(i)}{dt}\right)_{n+1}\right]\Delta t$$

This expression should give values of $Y_{n+1}(i)$ with residual errors of $O(\Delta t^3)$. For thermal quantities like T and $\rho_{\mathrm{e}+\gamma}$ one can calculate the time derivatives directly. But as (Wagoner, 1969) [7] noted the time derivatives for $Y(i)$ (Equation (2.4)) equal a proportionately small difference of two large numbers for high values of T. The equations for $dY(i)/dt$ are stiff. The book "Numerical Recipes in FORTRAN" [35] goes over the limitations of solving for $dY(i)/dt$

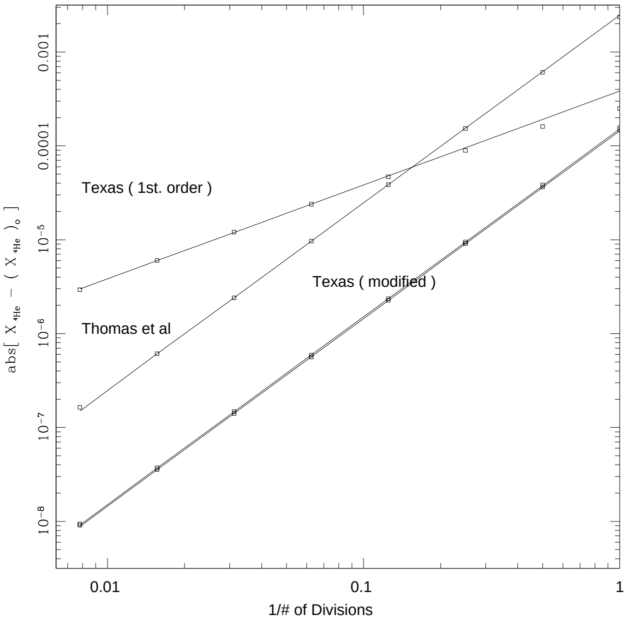

Figure 2.5: $X_{^4\mathrm{He}}$ in the Texas code at first has first order convergence vs the second order convergence of the Thomas et al code. The modifications in this section enable the Texas code to have second order convergence as well.

explicitly. Suppose the equation for $dY(i)/dt$ could be written in linearized form.

$$\frac{dY(i)}{dt} = -C_{ij} \times Y(j)$$

where C_{ij} is a positive definite matrix. Expanding from $Y_n(i)$ up to $Y_{n+1}(i)$ one gets

$$\begin{aligned} Y_{n+1}(i) &= Y_n(i) + \left(\frac{dY(i)}{dt}\right)_n \Delta t_n + \cdots \\ Y_{n+1}(i) &= (1 - \Delta t_n C_{ij}) \times Y_n(j) \end{aligned}$$

If Λ are the eigenvalues of $(1-\Delta t_n C_{ij})$ then Δt_n has to be smaller than $2/\Lambda_{max}$ in order for this solution to be stable. Whereas if one starts by expanding from $Y_{n+1}(i)$ down to $Y_n(i)$.

$$\begin{aligned} Y_n(i) &= Y_{n+1}(i) - \left(\frac{dY(i)}{dt}\right)_{n+1} \Delta t_n + \cdots \\ (1 - \Delta t_n C_{ij})^{-1} \times Y_n(i) &= Y_{n+1}(i) \end{aligned} \tag{2.28}$$

$(1 - \Delta t_n C_{ij})^{-1}$ has $1/(1 + \Lambda\Delta t)$ for eigenvalues, and these eigenvalues are always less than one regardless of the value of Δt. One has to apply Equation (2.28) to the two time derivatives in Equation (2.5).

Equation (2.28) provides a means of calculating the second of the time derivatives in Equation (2.5) in the Thomas et al code.

$$\frac{Y_{n+1}(i) - Y_n(i)}{\Delta t_n} = \left(\frac{dY(i)}{dt}\right)_{n+1} + \cdots \tag{2.29}$$

Rather than solve for $(dY(i)/dt)_{n+1}$ the Thomas et al code first solves for a $Y_{n+1}(i)$ that satisfies both sides of Equation (2.29). So the code defines $Y_{n\beta}(i)$ as that approximation of $Y_{n+1}(i)$ that does satisfy (2.29). But then the right hand side will be nonlinear in $Y_{n\beta}(i)$. The code linearizes it by replacing terms such as $Y_{n\beta}(i)Y_{n\beta}(j)$ with $1/2(\tilde{Y}_n(i)Y_{n\beta}(j) + Y_{n\beta}(i)\tilde{Y}_n(j))$ The interim $\tilde{Y}_n(i)$ is also an approximation of $Y_{n+1}(i)$. So the averaging between $\tilde{Y}_n(i)$ and $Y_{n\beta}(i)$ assumes that $\tilde{Y}_n(i)$, $Y_{n\beta}(i)$ and $Y_{n+1}(i)$ are all nearly equal to each other. The code replaces $Y_{n+1}(i)$ with $Y_{n\beta}(i)$ on the left hand side of (2.29), and the equation's final form is Equation (2.25).

$$\frac{Y_{n\beta}(i) - Y_n(i)}{\Delta t_n} = \sum_{i,j,k} -\frac{N_i[ij]}{N_i!N_j!(N_i + N_j)}$$

$$[N_i \tilde{Y}_n^{N_i-1}(i)\tilde{Y}_n^{N_j}(j)Y_{n\beta}(i) + N_j\tilde{Y}_n^{N_i}(i)\tilde{Y}_n^{N_j-1}(j)Y_{n\beta}(j)]$$
$$+\frac{N_i[kl]}{N_k!N_l!(N_k+N_l)}[N_k\tilde{Y}_n^{N_k-1}(k)\tilde{Y}_n^{N_l}(l)Y_{n\beta}(k) +$$
$$N_l\tilde{Y}_n^{N_k}(k)\tilde{Y}_n^{N_l-1}(l)Y_{n\beta}(l)]$$

What about the first time derivative in (2.5)? To solve for that time derivative start by expanding from $Y_n(i)$ down to $Y_{n-1}(i)$.

$$\begin{aligned} Y_{n-1}(i) &= Y_n(i) - \left(\frac{dY(i)}{dt}\right)_n \Delta t_{n-1} + \cdots \qquad (2.30) \\ \frac{Y_n(i) - Y_{n-1}(i)}{\Delta t_{n-1}} &= \left(\frac{dY(i)}{dt}\right)_n + \cdots \end{aligned}$$

Replace $Y_n(i)$ with $Y_{n\alpha}(i)$ which one must solve for. On the right hand side replace $Y_{n\alpha}(i)Y_{n\alpha}(j)$ with $1/2(Y_n(i)Y_{n\alpha}(j) + Y_{n\alpha}(i)Y_n(j))$, an average between $Y_{n\alpha}(i)$ and $Y_n(i)$, the latter term which is already known. The final form is then Equation (2.19).

$$\begin{aligned} \frac{Y_{n\alpha}(i) - Y_{n-1}(i)}{\Delta t_{n-1}} &= \sum_{i,j,k} -\frac{N_i[ij]}{N_i!N_j!(N_i+N_j)} \\ &[N_i Y_n^{N_i-1}(i)Y_n^{N_j}(j)Y_{n\alpha}(i) + N_j Y_n^{N_i}(i)Y_n^{N_j-1}(j)Y_{n\alpha}(j)] \\ &+\frac{N_i[kl]}{N_k!N_l!(N_k+N_l)}[N_k Y_n^{N_k-1}(k)Y_n^{N_l}(l)Y_{n\alpha}(k) + \\ &N_l Y_n^{N_k}(k)Y_n^{N_l-1}(l)Y_{n\alpha}(l)] \end{aligned}$$

Plugging in the left hand sides of (2.19) and (2.25) into (2.5), this author gets the following expression for $Y_{n+1}(i)$ in the Thomas et al code.

$$Y_{n+1}(i) = Y_n(i) + \frac{1}{2}\left[\frac{Y_{n\alpha}(i) - Y_{n-1}(i)}{\Delta t_{n-1}} + \frac{Y_{n\beta}(i) - Y_n(i)}{\Delta t_n}\right]\Delta t_n$$

n	T	Y_n	$Y_{n\alpha}$	% difference
142	0.9007	$3.38710889 \times 10^{-4}$	$3.42315019 \times 10^{-4}$	1.0641
143	0.8978	$3.92797048 \times 10^{-4}$	$3.96859336 \times 10^{-4}$	1.0342
144	0.8950	$4.54696110 \times 10^{-4}$	$4.59267855 \times 10^{-4}$	1.0055
145	0.8922	$5.25426339 \times 10^{-4}$	$5.30563544 \times 10^{-4}$	0.9777
146	0.8895	$6.06125679 \times 10^{-4}$	$6.11889426 \times 10^{-4}$	0.9509
147	0.8868	$6.98064311 \times 10^{-4}$	$7.04520801 \times 10^{-4}$	0.9249
148	0.8842	$8.02658511 \times 10^{-4}$	$8.09879389 \times 10^{-4}$	0.8996
149	0.8816	$9.21485763 \times 10^{-4}$	$9.29548143 \times 10^{-4}$	0.8749
150	0.8790	$1.05630132 \times 10^{-3}$	$1.06528809 \times 10^{-3}$	0.8508

n	T	$\tilde{Y}_n$	$Y_{n\beta}$	% difference
142	0.8978	$3.88897120 \times 10^{-4}$	$3.96696975 \times 10^{-4}$	2.0056
143	0.8950	$4.50302048 \times 10^{-4}$	$4.59090171 \times 10^{-4}$	1.9516
144	0.8922	$5.20483048 \times 10^{-4}$	$5.30369631 \times 10^{-4}$	1.8995
145	0.8895	$6.00572904 \times 10^{-4}$	$6.11678455 \times 10^{-4}$	1.8492
146	0.8868	$6.91836464 \times 10^{-4}$	$7.04292158 \times 10^{-4}$	1.8004
147	0.8842	$7.95684405 \times 10^{-4}$	$8.09632617 \times 10^{-4}$	1.7530
148	0.8816	$9.13688431 \times 10^{-4}$	$9.29283094 \times 10^{-4}$	1.7068
149	0.8790	$1.04759783 \times 10^{-3}$	$1.06500481 \times 10^{-3}$	1.6616
150	0.8765	$1.19935764 \times 10^{-3}$	$1.21875540 \times 10^{-3}$	1.6173

Table 2.4: $Y(^4\text{He})$ in the Thomas et al code, $\eta_{10} = 3.0$. (2.4a) lists Y_n and $Y_{n\alpha}$ from the first Runge-Kutta step, and the absolute difference between $Y_{n\alpha}$ and Y_n as a percentage of Y_n. (2.4b) lists $\tilde{Y}_n$ and $Y_{n\beta}$ from the second Runge-Kutta step, and the percent difference between $Y_{n\beta}$ and $\tilde{Y}_n$. Note the small values of the percent differences.

Table (2.4a) lists actual values of $Y_n(^4\text{He})$ and $Y_{n\alpha}(^4\text{He})$ and Table (2.4b) lists $\tilde{Y}_n(^4\text{He})$ and $Y_{n\beta}(^4\text{He})$ for $T =$ around 0.9 GK. At this point in the run $Y_{n+1}(^4\text{He})$ differs from $Y_n(^4\text{He})$ by around 16 %. In comparison $Y_{n\alpha}(^4\text{He})$ differs from $Y_n(^4\text{He})$ by only 1 % while $Y_{n\beta}(^4\text{He})$ differs from $\tilde{Y}_n(^4\text{He})$ by 2 %.

The Texas code's Equation (2.12) for the second R-K time derivative is equivalent to Equation (2.25) for the Thomas et al code. (Except that (2.12) uses the final value T_{n+1} instead of the interim value $\tilde{T}_n$ of (2.25) to calculate reaction rates. But $\tilde{T}_n$ is an approximation of T_{n+1} and so this difference shouldn't affect the results very much.) But Equation (2.6) (rewritten below), the Texas code's equation for the first R-K time derivative, doesn't make sense compared with the Thomas et al code's Equation (2.19).

$$\begin{aligned}\frac{Y_{n\alpha}(i) - Y_n(i)}{\Delta t_n} &= \sum_{i,j,k} -\frac{N_i[ij]}{N_i!N_j!(N_i+N_j)} \\ &\quad [N_i Y_n^{N_i-1}(i) Y_n^{N_j}(j) Y_{n\alpha}(i) + N_j Y_n^{N_i}(i) Y_n^{N_j-1}(j) Y_{n\alpha}(j)] \\ &\quad + \frac{N_i[kl]}{N_k!N_l!(N_k+N_l)}[N_k Y_n^{N_k-1}(k) Y_n^{N_l}(l) Y_{n\alpha}(k) + \\ &\quad N_l Y_n^{N_k}(k) Y_n^{N_l-1}(l) Y_{n\alpha}(l)]\end{aligned}$$

The left hand side of Equation (2.6) is the same as that of Equation (2.12). That would imply that the Texas code's $Y_{n\alpha}(i)$ is an approximation of $Y_n(i)$ instead of $Y_{n-1}(i)$. That would mean that the right hand side is a mix of $Y_n(i)$ and an approximation of $Y_{n+1}(i)$. Table (2.5a) lists $Y_n(^4\mathrm{He})$ and $Y_{n\alpha}(^4\mathrm{He})$ and Table (2.5b) lists $\tilde{Y}_n(^4\mathrm{He})$ and $Y_{n\beta}(^4\mathrm{He})$ for the Texas code at the same temperature range as in Tables (2.4a) and (2.4b). Because the Texas code has much shorter timestep differences than the Thomas et al code has, $Y_{n+1}(i)$ differs from $Y_n(i)$ by about 2.7 % at $T = 0.9$ GK, vs 16 % for the Thomas et al code. But the Texas code's $Y_{n\alpha}(i)$ differs from $Y_n(i)$ by 2.7 % as well. In comparison the Texas code's $Y_{n\beta}(i)$ differs from $\tilde{Y}_n(i)$ by only 0.04 %. At any timestep n, $Y_{n\alpha}(i)$ is in fact closer to $Y_{n+1}(i)$ than $Y_n(i)$.

Plug in the left hand sides of Equations (2.6) and (2.12) into Equation (2.5).

$$\tilde{Y}_n(i) = Y_n(i) + \frac{Y_{n\alpha}(i) - Y_n(i)}{\Delta t_n}\Delta t_n$$

n	T	Y_n	$Y_{n\alpha}$	% difference
1315	0.9009	$3.33714194 \times 10^{-4}$	$3.42714502 \times 10^{-4}$	2.6970
1316	0.9003	$3.42788546 \times 10^{-4}$	3.5202754×10^{-4}	2.6952
1317	0.8998	$3.52103438 \times 10^{-4}$	$3.61587275 \times 10^{-4}$	2.6935
1318	0.8993	$3.61665073 \times 10^{-4}$	$3.71400062 \times 10^{-4}$	2.6917
1319	0.8988	$3.71479805 \times 10^{-4}$	$3.81472415 \times 10^{-4}$	2.6899
1320	0.8983	$3.81554149 \times 10^{-4}$	3.9181101×10^{-4}	2.6882
1321	0.8977	$3.91894783 \times 10^{-4}$	$4.02422691 \times 10^{-4}$	2.6864
1322	0.8972	$4.02508551 \times 10^{-4}$	$4.13314472 \times 10^{-4}$	2.6846
1323	0.8967	$4.13402469 \times 10^{-4}$	$4.24493541 \times 10^{-4}$	2.6829

n	T	$\tilde{Y}_n$	$Y_{n\beta}$	% difference
1315	0.9003	$3.42714502 \times 10^{-4}$	$3.42862589 \times 10^{-4}$	0.0432
1316	0.8998	$3.52027540 \times 10^{-4}$	$3.52179337 \times 10^{-4}$	0.0431
1317	0.8993	$3.61587275 \times 10^{-4}$	$3.61742871 \times 10^{-4}$	0.0430
1318	0.8988	$3.71400062 \times 10^{-4}$	$3.71559548 \times 10^{-4}$	0.0429
1319	0.8983	$3.81472415 \times 10^{-4}$	$3.81635883 \times 10^{-4}$	0.0429
1320	0.8977	$3.91811010 \times 10^{-4}$	$3.91978556 \times 10^{-4}$	0.0428
1321	0.8972	$4.02422691 \times 10^{-4}$	$4.02594412 \times 10^{-4}$	0.0427
1322	0.8967	$4.13314472 \times 10^{-4}$	$4.13490466 \times 10^{-4}$	0.0426
1323	0.8962	$4.24493541 \times 10^{-4}$	$4.24673911 \times 10^{-4}$	0.0425

Table 2.5: $Y(^4\text{He})$ in the Texas et al code, $\eta_{10} = 3.0$. (2.5a) and (2.5b) are the same as Tables (2.4a) and (2.4b) of the Thomas et al code. The percent differences are much larger in Table (2.5a) then in Table (2.5b). $Y_{n\alpha}$ seems closer to Y_{n+1} than Y_n.

$$\begin{aligned}
\tilde{Y}_n(i) &= Y_{n\alpha}(i) \\
Y_{n+1}(i) &= Y_n(i) + \frac{1}{2}\left[\frac{Y_{n\alpha}(i) - Y_n(i)}{\Delta t_n} + \frac{Y_{n\beta}(i) - Y_n(i)}{\Delta t_n}\right]\Delta t_n \\
Y_{n+1}(i) &= \frac{1}{2}(Y_{n\alpha}(i) + Y_{n\beta}(i)) \qquad (2.31)
\end{aligned}$$

Because of the use of Δt_n and $Y_n(i)$ in the first time derivative, the interim $\tilde{Y}_n(i)$ equals $Y_{n\alpha}(i)$, the $Y(i)$ calculated by solving the matrix equation. Further, the final value of $Y_{n+1}(i)$ equals the average of $Y_{n\alpha}(i)$ and $Y_{n\beta}(i)$, which in the Texas code are both first-order approximations of $Y_{n+1}(i)$ calculated from the matrix equations alone.

(Note: One other error that the Texas code's equation for the first R-K time derivative has is for 2+1 reactions [36]

$$^{A_i}Z_i +^{A_j} Z_j \quad \leftrightarrow \quad ^{A_k}Z_k + \gamma$$

The term in Equation (2.4) corresponding to this reaction is

$$\frac{dY(i)}{dt} \quad = \quad -Y(i)Y(j)[ij] + Y(k)[kl]$$

Both codes replace the $Y(k)$ in the positive term with $Y_{n\alpha}(k)$

$$Y_n(k)[kl] \quad \rightarrow \quad Y_{n\alpha}(k)[kl]$$

for Equations (2.6) and (2.19). In the Thomas et al code, that term is originally $Y_n(k)[kl]$ a term already linear in $Y_n(k)$. The right hand side of Equation (2.19) is made up of $Y_n(i)$ and $Y_{n\alpha}(i)$ which is an approximation of $Y_n(i)$. So there's no ambiguity in using just $Y_{n\alpha}(k)$ for the 2+1 reaction's positive term. But in the right hand side of Equation (2.6) $Y_{n\alpha}(i)$ is more equal to $Y_{n+1}(i)$. All terms in Equation (2.6) should use both $Y_n(i)$ and $Y_{n\alpha}(i)$ in order for the Texas code to run accurately, but these 2+1 terms use only $Y_{n\alpha}(i)$.)

This author first changed the Texas code's first R-K step so that it would use $Y_{n-1}(i)$ and Δt_{n-1} instead of $Y_n(i)$ and Δt_n, but didn't change the point in a run where the Texas code calculated Δt_n, or the use of final values of the reaction rates instead of interim values in the second R-K step.

Table (2.6a) lists $Y_n(^4\text{He})$ and $Y_{n\alpha}(^4\text{He})$ and Table (2.6b) lists $\tilde{Y}_n(^4\text{He})$ and $Y_{n\beta}(^4\text{He})$ for this version of the Texas code. $Y_{n\alpha}(i)$ now differs from $Y_n(i)$,

n	T	Y_n	$Y_{n\alpha}$	% difference
1320	0.9007	$3.39268273 \times 10^{-4}$	$3.39388950 \times 10^{-4}$	0.0356
1321	0.9002	$3.48493675 \times 10^{-4}$	$3.48617385 \times 10^{-4}$	0.0355
1322	0.8997	$3.57963587 \times 10^{-4}$	$3.58090403 \times 10^{-4}$	0.0354
1323	0.8992	$3.67684311 \times 10^{-4}$	$3.67814308 \times 10^{-4}$	0.0354
1324	0.8986	$3.77662303 \times 10^{-4}$	$3.77795558 \times 10^{-4}$	0.0353
1325	0.8981	$3.87904184 \times 10^{-4}$	$3.88040774 \times 10^{-4}$	0.0352
1326	0.8976	$3.98416738 \times 10^{-4}$	$3.98556743 \times 10^{-4}$	0.0351
1327	0.8971	$4.09206918 \times 10^{-4}$	$4.09350421 \times 10^{-4}$	0.0351
1328	0.8966	$4.20281854 \times 10^{-4}$	$4.20428937 \times 10^{-4}$	0.0350

n	T	$\tilde{Y}_n$	$Y_{n\beta}$	% difference
1320	0.9002	$3.48370867 \times 10^{-4}$	$3.48616483 \times 10^{-4}$	0.0705
1321	0.8997	$3.57837693 \times 10^{-4}$	$3.58089482 \times 10^{-4}$	0.0704
1322	0.8992	$3.67555256 \times 10^{-4}$	$3.67813366 \times 10^{-4}$	0.0702
1323	0.8986	$3.77530012 \times 10^{-4}$	$3.77794595 \times 10^{-4}$	0.0701
1324	0.8981	$3.87768578 \times 10^{-4}$	$3.88039790 \times 10^{-4}$	0.0699
1325	0.8976	$3.98277737 \times 10^{-4}$	$3.98555738 \times 10^{-4}$	0.0698
1326	0.8971	$4.09064442 \times 10^{-4}$	$4.09349395 \times 10^{-4}$	0.0697
1327	0.8966	$4.20135819 \times 10^{-4}$	$4.20427889 \times 10^{-4}$	0.0695
1328	0.8960	$4.31499172 \times 10^{-4}$	$4.31798529 \times 10^{-4}$	0.0694

Table 2.6: The same as in Tables (2.5a) and (2.5b), but now the equations for the first R-K time derivative has changed so that it uses Y_n and Δt_{n-1} like in the Thomas et al code. $Y_{n\alpha}$ is now closer to Y_n than Y_{n+1}.

by only 0.035 %. $Y_{n\beta}(i)$ differs form $\tilde{Y}_n(i)$ by a slightly higher percentage than before, 0.07 %. The convergence of $X_{^4\mathrm{He}}$ now obeys this second-order equation.:

$$X_{^4\mathrm{He}} = 0.2391419137 - (0.1445966603 \times 10^{-3})d^2$$

At $d = 1$ $X_{^4\mathrm{He}}$ has decreased from 0.2393922575 to 0.2389929572, and $X_{^4\mathrm{He}}$ now increases upward towards its convergent value like in the Thomas et al code. But $X_{^4\mathrm{He}}$ has nearly the same convergent value that it had when the code was first order.

This author then changed the Texas code so that it did calculate Δt_n at the same point in the run as the Thomas et al code, and use the interim values of the reaction rates. This version of the Texas code was used for the rest of the dissertation. The equation for the convergence then became:

$$X_{^4\mathrm{He}} = 0.2391419139 - (0.1512644560 \times 10^{-3})d^2$$

$X_{^4\mathrm{He}}$ changes only from 0.2389929572 to 0.2389856624. This author has noted that the interim abundance $\tilde{Y}_n(i)$ approximately equals the final abundance $Y_{n+1}(i)$. The interim reaction rate $[ij](\tilde{T}_n)$ is similarly close to the final rate $[ij](T_{n+1})$, close enough so that the choice of which of these two values to use in the second R-K step has little effect on $Y_{n+1}(i)$. This change in the Texas code's means of calculating Δt increased the number of timesteps only from 2791 to 2793, too small an increase to make a difference in the final value.

Either way, $X_{^4\mathrm{He}}$ still disagrees considerably with the Thomas et al code's $X_{^4\mathrm{He}} = 0.2367002863$. The next section discusses modifications to the Thomas et al code that can bring the codes in agreement with each other.

2.3 The Value of Y_{min}

To calculate Δt_n the Thomas et al code used Equation (2.21) (repeated below),

$$\Delta t_n = dk \min\left[\frac{Y_n(i)}{\dot{Y}_n(i)} dk_{\mathrm{fac}}, \frac{T_n}{\frac{dT}{dt}}\right]$$

$Y_{\rm min}$	Thomas et al	Thomas et al (0.1)	Texas	Texas (0.1)
10^{-25}	325	1009	312	1030
10^{-35}	469	1033	455	1051
10^{-45}	560	1055	543	1069
10^{-55}	621	1078	589	1088
10^{-65}	701	1110	684	1118
10^{-75}	804	1159	787	1164
10^{-85}	913	1218	896	1220
10^{-95}	1020	1287	1004	1286
0.0	2781	2882	2772	2879
0.0 (dk_{fac})	1067	1321	1050	1320

Table 2.7: The number of timesteps both codes take for a run using the Thomas et al code's method of calculating Δt, both with and without the 0.1 factor on $T/(dT/dt)$ or $4\rho_{\rm e+\gamma}/(d\rho_{\rm e+\gamma}/dt)$

$$\begin{aligned} dk_{\rm fac} &= \left(1 + \left(-\frac{\log Y_n(i)}{dt_{\rm fac}}\right)^2\right) \\ dt_{\rm fac} &= -\frac{\log Y_{\rm min}}{\frac{dk_{\rm max}}{dk} - 1} \end{aligned}$$

which has a dependence on $Y_{\rm min}$. So this author varied the value of $Y_{\rm min}$ to see how $Y_{\rm min}$ affects a run. This author also had the Thomas et al code run without the $dt_{\rm fac}$ factor for the case $Y_{\rm min}$ =0.0. In that case the Thomas et al code could mimick the behavior of the Texas code. Figure (2.6a) shows the values of Δt for several values of $Y_{\rm min}$, and the second column in Table (2.7) lists the number of timesteps in each of the Thomas et al code's runs.

All the graphs in Figure (2.6a) behave linearly at near the highest temperatures. In this region the ratio $T/(dT/dt)$ determines the value of Δt. The graphs with $Y_{\rm min} < 10^{-25}$ break from the linear behavior when the ratio $[dk_{\rm fac}Y(^4{\rm He})]/[dY(^4{\rm He})/dt]$ falls below the ratio for T. $dk_{\rm fac}$ makes the ^{4}He ratio so big for $Y_{\rm min} = 10^{-25}$ that its graph doesn't bend until much later than the other graphs. The factor also makes the ratio smaller and smaller

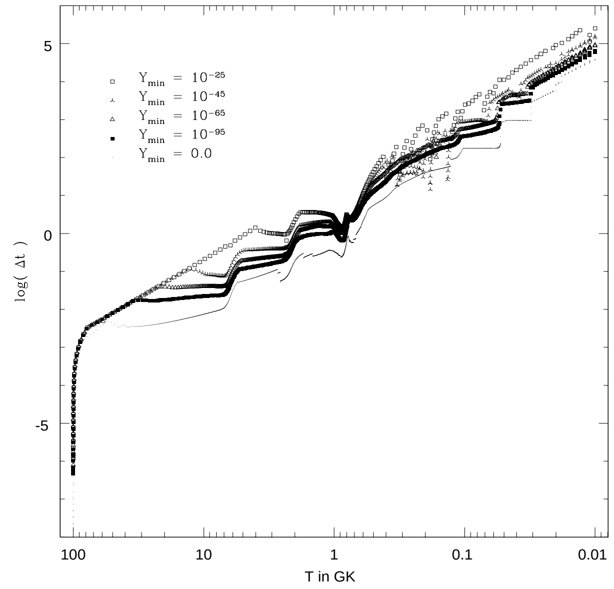

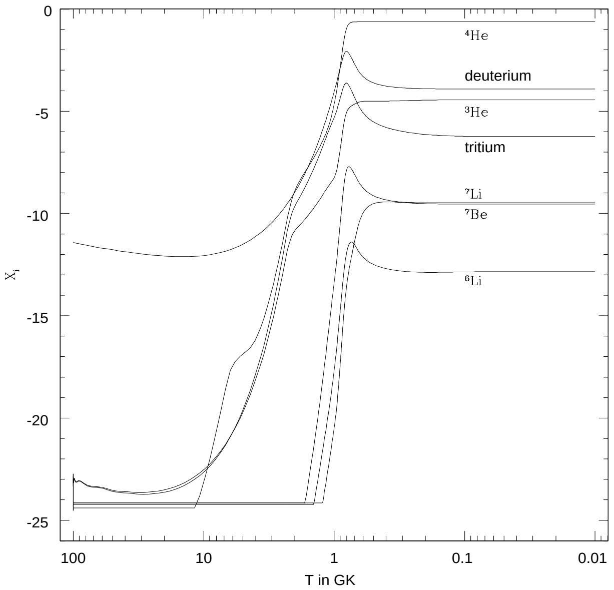

Figure 2.6: In (2.6a) the number of timesteps increases with decreasing value of Y_{min}. The structures in these graphs can be matched to the graphs for the mass fractions in (2.6b). Both graphs are for the Thomas et al code at $\eta_{10} = 3.0$.

with decreasing Y_{min}, and the graphs bend at higher temperatures. One can then match up Figure (2.6a) with the mass fractions shown in Figure (2.6b) to explain the various dents in the graphs. ^{4}He falls out of NSE with ^{3}He and tritium at around $T = 8$ GK. The time derivative of $Y(^4\mathrm{He})$ decreases at 8 GK leading to the increase in Δt. At 5 GK, $[dk_{\mathrm{fac}}Y(\mathrm{t})]/[dY(\mathrm{t})/dt]$ gets lower than the ratio for ^{4}He and Δt briefly levels off. Tritium falls out of NSE with deuterium at 2 GK and so Δt increases before levelling off again when deuterium starts determining its value. Finally, big bang nucleosynthesis occurs when deuterium falls out of NSE with free neutrons and protons at 0.9 GK. ^{4}He determines Δt when deuterium starts falling, and Δt dips until $Y(^4\mathrm{He})$ reaches its final value. For lower temperatures several of the heavier isotopes determine the details in the graphs.

As Y_{min} reduces by a factor of 10^{-10} the number of timesteps increases by around 100, reaching 1020 when $Y_{\mathrm{min}} = 10^{-95}$. For the case in Figure (2.6a) where $Y_{\mathrm{min}} = 0.0$ Equation (2.21) doesn't have the dk_{fac} factor. Without that factor $Y(i)/[dY(i)/dt]$ falls in value an order of four or five, and the number of timesteps jumps to 2781, a number comparable to the number of timesteps the Texas code uses. Also, $X_{^4\mathrm{He}}$ in this case equals 0.2390586572, less than 10^{-6} different from $X_{^4\mathrm{He}}$'s convergent value. Figure (2.7) shows $X_{^4\mathrm{He}}$ as a function of Y_{min} and shows $X_{^4\mathrm{He}}$ for $Y_{\mathrm{min}} = 0.0$ for comparison. At the lowest values of Y_{min} $X_{^4\mathrm{He}}$ seems to converge to a final value. But there appeared to be no strong linear relationship between $X_{^4\mathrm{He}}$ and either Y_{min} or the number of timesteps.

When $T/(dT/dt)$ determines Δt the graphs in Figure (2.6a) behave smoothly and have fewer timesteps than in the regions where the abundances determine Δt. Lowering $T/(dT/dt)$ enough so that it determines Δt for most

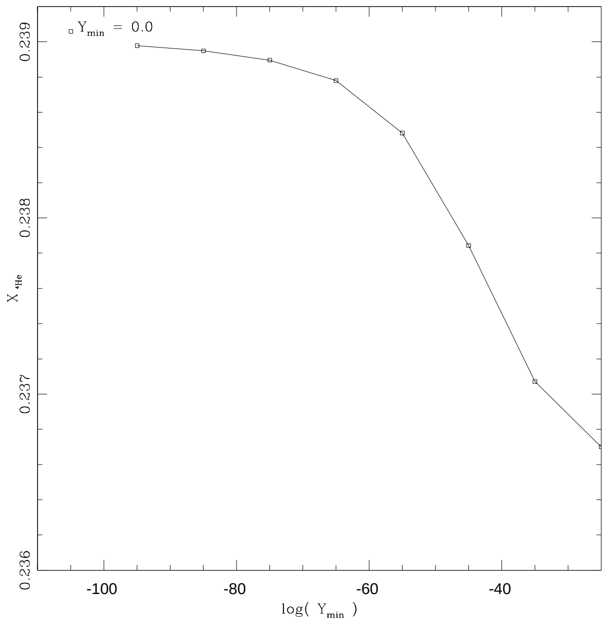

Figure 2.7: $X_{^4\mathrm{He}}$ approaches its ($Y_{\mathrm{min}} = 0.0$) value as Y_{min} decreases, but this graph apparently doesn't obey a particular function.

of the run leads to a linear graph. This author then puts an extra factor 0.1 onto $T/(dT/dt)$. Figure (2.8) shows that for $Y_{\mathrm{min}} = 10^{-25}$ $0.1T/(dT/dt)$ is considerably lower than $[dk_{\mathrm{fac}}Y(i)]/[dY(i)/dt]$ except around $T = 1$ GK, when the ratio for ^{4}He is still lower. The code now runs in 1009 steps. Table (2.7) shows that the number of timesteps varies between 1000 and 1300, a smaller range than without the 0.1 factor but more timesteps than the previous runs. Figure (2.9) shows that the graphs from Figure (2.6a) are far less varied. And in Figure (2.10) the 0.1 factor has reduced the variation of $X_{^4\mathrm{He}}$ with respect to Y_{min} to only an order of 10^{-6}. These results indicate that the number of timesteps and not Y_{min} determines the final $X_{^4\mathrm{He}}$ in the Thomas et al Code, and that this code needs to run at least 1000 steps in order to produce an $X_{^4\mathrm{He}}$

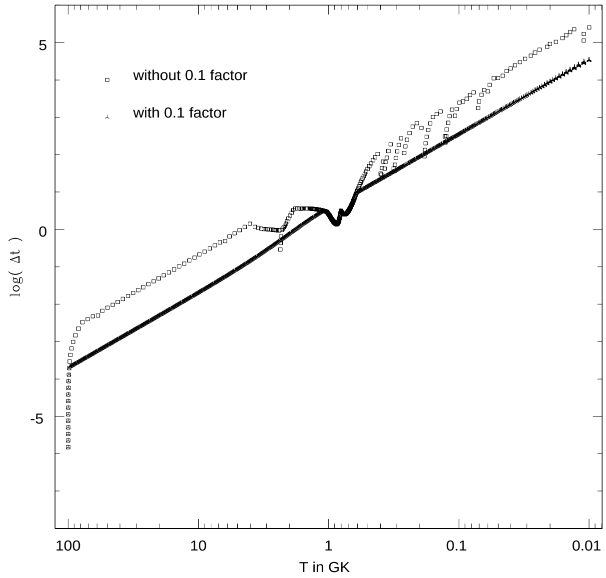

Figure 2.8: A factor of 0.1 put on the ratio $T/(dT/dt)$ makes the graph for Δt much more linear. Here $Y_{\min} = 10^{-25}$.

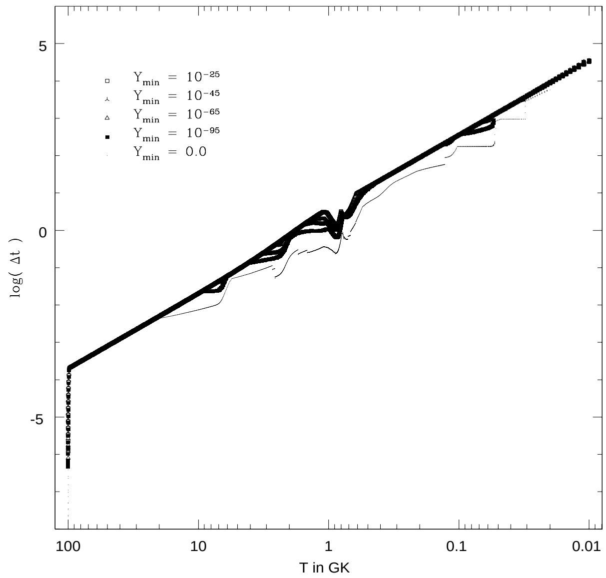

Figure 2.9: Δt in the Thomas et al code at $\eta_{10} = 3.0$, now with the 0.1 factor on $T/(dT/dt)$.

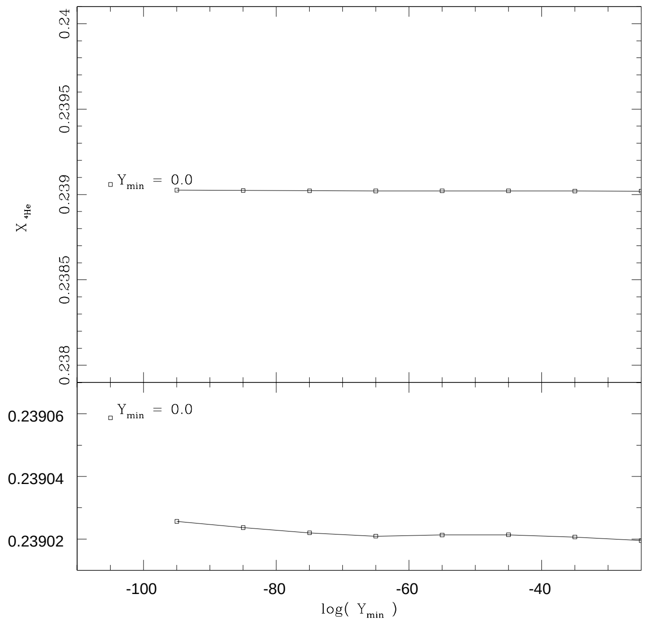

Figure 2.10: With the 0.1 factor $X_{^4\mathrm{He}}$ has much less dependence on the value of Y_{min}.

within 0.0001 of its convergent value.

This author modified Equation (2.14) in the Texas code so that its ratio $Y(i)/[dY(i)/dt]$ would have a dk_{fac} factor as well. For the Texas code to recreate the same results as in the Thomas et al code, the ratio $\rho_{\mathrm{e}+\gamma}/(d\rho_{\mathrm{e}+\gamma}/dt)$ had to be multiplied by 4.

$$4\frac{\rho_{\mathrm{e}+\gamma}}{\dot{\rho}_{\mathrm{e}+\gamma}} \approx \frac{T}{\dot{T}}$$

At the highest temperatures both ρ_{e} and ρ_γ would have a T^4 dependence, and at the lowest ρ_{e} would nearly approach zero. Of course this equation wasn't accurate for the temperatures in between, but it was still a good approximation.

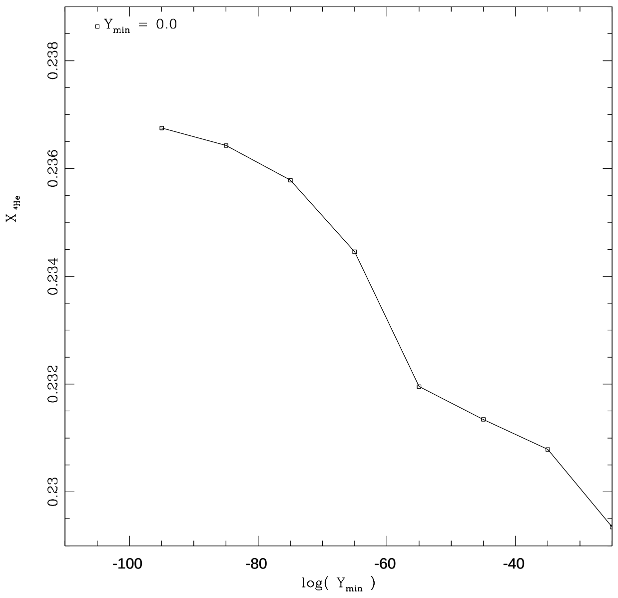

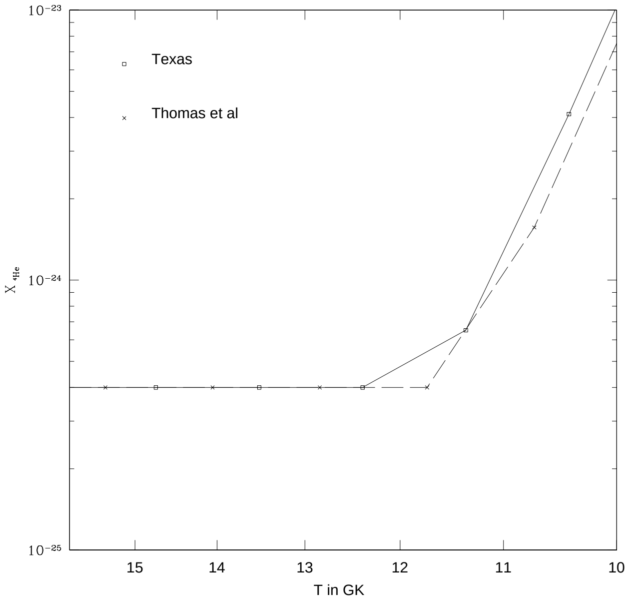

Figure 2.11: (2.11a) shows that the Texas code has a stronger dependence on the number of timesteps (varied by varying $Y_{\min}$) than the Thomas et al code. (2.11b) and (2.11c) show closeups of $X_{^4\mathrm{He}}$ for both codes, showing how $X_{^4\mathrm{He}}$ comes out less in the Texas code for $Y_{\min} = 10^{-25}$.

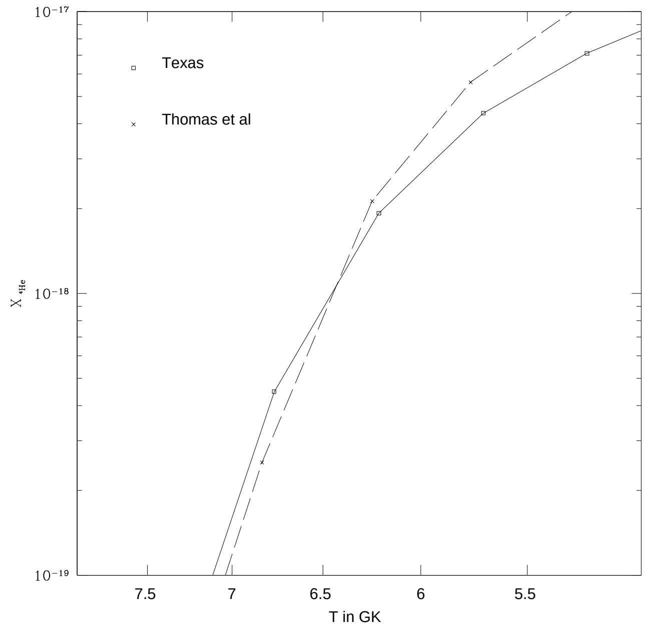

With this modification the Texas code exhibits behavior similar to the Thomas et al Code. The third column in Table (2.7) lists the number of timesteps the Texas code uses for its runs, and the number is always comparable to the Thomas et al code's number. But the reduced number of timesteps has a considerably larger influence on the Texas code than on the Thomas et al code. Figure (2.11a) shows that a nonzero Y_{min} reduces $X_{^4\mathrm{He}}$ by as much as 0.009 for $Y_{\mathrm{min}} = 10^{-25}$, and not until $Y_{\mathrm{min}} = 10^{-95}$ does $X_{^4\mathrm{He}}$ equal the Thomas et al code's $X_{^4\mathrm{He}}$ at $Y_{\mathrm{min}} = 10^{-25}$. Figures (2.11b) and (2.11c) show how $X_{^4\mathrm{He}}$ of both codes depends on T for the case of $Y_{\mathrm{min}} = 10^{-25}$. $X_{^4\mathrm{He}}$ breaks from its minimum value of 4×10^{-25} at nearly the same time in both codes. But at that same time, the temperature is lower in the Thomas et al code than the Texas code. The graphs for $X_{^4\mathrm{He}}$ break at different points in Figure (2.11b). An isotope in NSE will have a higher derivative with respect to temperature the lower the temperature. So $X_{^4\text{He}}$ increases more rapidly in the Thomas et al code than the Texas code. But the Texas code's $X_{^4\text{He}}$ starts increasing at a temperature higher enough to be still larger than the Thomas et al code's $X_{^4He}$ at first. But Figure (2.11c) shows that the Texas code's $X_{^4\text{He}}$ falls below the Thomas et al code's $X_{^4\text{He}}$ when ^{4}He falls out of NSE with ^{3}He and tritium, and it stays below the Thomas et al code's $X_{^4\text{He}}$ from then on.

Multiplying $\rho_{e+\gamma}/(d\rho_{e+\gamma}/dt)$ by 0.1 has the same effect on the Texas code that the 0.1 factor does on the Thomas et al code. Figure (2.13) shows $X_{^4\text{He}}$'s considerable reduction in dependence on Y_{min} due to the 0.1 factor. Between $Y_{\text{min}} = 10^{-25}$ and 10^{-95} $X_{^4\text{He}}$ increases by 6×10^{-6} for the Thomas et al code and 39×10^{-6} in the Texas code. So the Texas code still has a larger dependence, but a dependence an order of magnitude less than 10^{-4}.

This author would prefer to not have an artificial non-zero value of Y_{min} at all. Suggested by the Thomas et al code's means of calculating Δt one can define dk_{fac} for the case of $Y_{\text{min}} = 0.0$ as

$$
\begin{aligned}
dk_{\text{fac}} &= \left(1 + \left(-\frac{\log Y_n(i)}{dt_{\text{fac}}}\right)^2\right) \\
dt_{\text{fac}} &= -\frac{\log 10^{-99}}{\frac{dk_{\text{max}}}{dk} - 1}
\end{aligned}
$$

dk_{fac} by itself reduces the number of timesteps from 2772 down to 1050. Figure (2.14) shows that with dk_{fac} included Δt is determined by $\rho_{e+\gamma}$ down to a much lower temperature than without it. The Texas code yields a final value of $X_{^4\text{He}} = 0.2368480125$. Considerably lower than $X_{^4\text{He}} = 0.2390899458$ without dk_{fac} but more consistent with the values of $X_{^4\text{He}}$ for non-zero Y_{min} Finally when both dk_{fac} and the 0.1 factor are included, the Texas code runs in

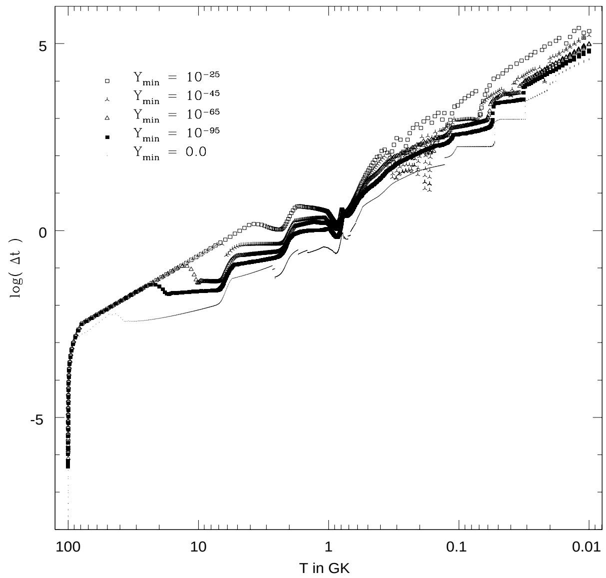

Figure 2.12: Δt as a function of temperature for the Texas code, for various values of Y_{min}.

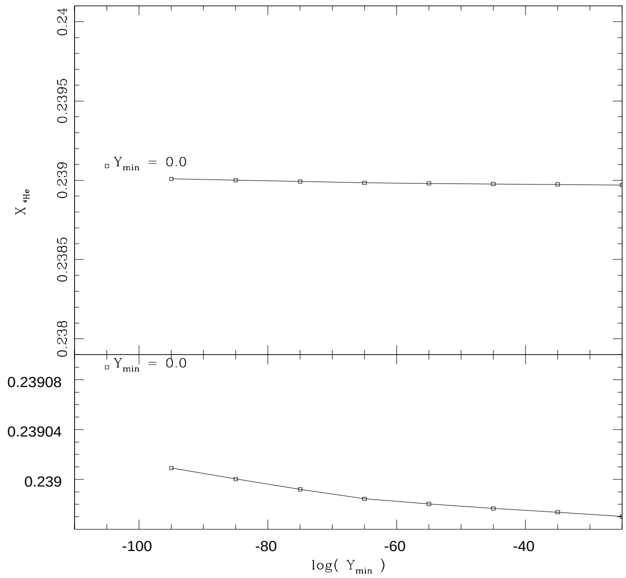

Figure 2.13: With the 0.1 factor $X_{^4\mathrm{He}}$ has much less dependence on the value of Y_{min}.

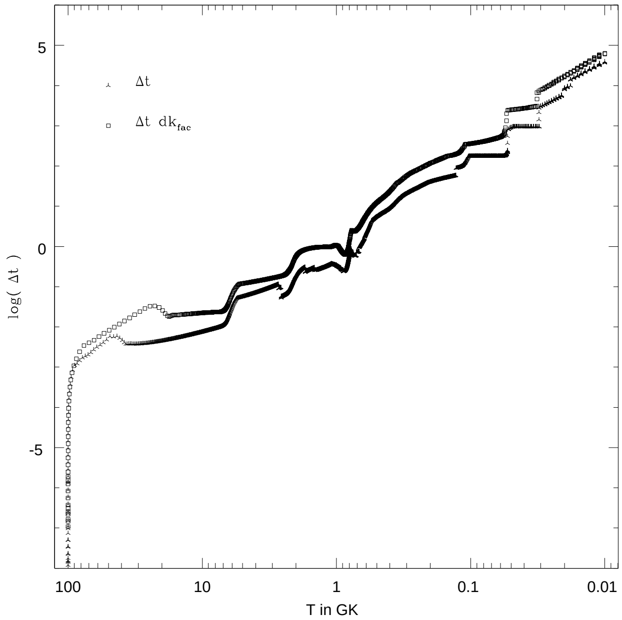

Figure 2.14: The $dk_{\rm fac}$ factor defined to work for $Y_{\rm min}$ reduces the number of timesteps in the Texas code from 2772 to 1050.

1320 timesteps and yields a final value of $X_{^4\rm He} = 0.2390197529$. This author has put in the 0.1 factor and $dk_{\rm fac}$ for $Y_{\rm min} = 0.0$ into the Thomas et al code. That code then runs in 1321 timesteps with a final $X_{^4\rm He} = 0.2390335785$. Finally both codes agree to less than 10^{-4} and run with a manageable number of timesteps.

2.4 Final Results

Table (2.8) lists the codes' final mass fractions for ^{4}He and various other isotopes for the case of $\eta_{10} = 3.0$ and $Y_{\rm min} = 0.0$. As a whole, the mass fractions have better agreement with each other than in Table (2.3). The mass frac-

isotope	Thomas et al X	Texas X
n	$0.511929622 \times 10^{-15}$	$0.5260113927 \times 10^{-15}$
p	0.7608082624	0.7608212397
d	$0.1214184526 \times 10^{-3}$	$0.1221710298 \times 10^{-3}$
^{3}H	$0.5868014199 \times 10^{-6}$	$0.590369871 \times 10^{-6}$
^{3}He	$0.361533069 \times 10^{-4}$	$0.3624558721 \times 10^{-4}$
^{4}He	0.2390335785	0.2390197529
^{6}Li	$0.1450455199 \times 10^{-12}$	$0.1459037629 \times 10^{-12}$
^{7}Li	$0.3420326438 \times 10^{-9}$	$0.3438609857 \times 10^{-9}$
^{7}Be	$0.2810839353 \times 10^{-9}$	$0.2773688629 \times 10^{-9}$
^{9}Be	$0.1076149005 \times 10^{-16}$	$0.1089000217 \times 10^{-16}$
^{10}B	$0.9314300115 \times 10^{-18}$	$0.9389613021 \times 10^{-18}$
^{11}B	$0.9855051922 \times 10^{-16}$	$0.9596388952 \times 10^{-16}$
^{12}C	$0.3015779708 \times 10^{-13}$	$0.2997099492 \times 10^{-13}$
^{13}C	$0.205797869 \times 10^{-14}$	$0.2034295405 \times 10^{-14}$
^{14}C	$0.649489058 \times 10^{-13}$	$0.6477522031 \times 10^{-13}$
^{14}N	$0.1318121059 \times 10^{-12}$	$0.1314743162 \times 10^{-12}$
^{16}O	$0.7643550113 \times 10^{-17}$	$0.758611841 \times 10^{-17}$
^{19}F	$0.7490196973 \times 10^{-24}$	$0.7429878858 \times 10^{-24}$
^{20}F	$0.3448046117 \times 10^{-24}$	$0.3519348336 \times 10^{-24}$
^{21}Ne	$0.535591721 \times 10^{-23}$	$0.532430875 \times 10^{-23}$

Table 2.8: With this chapter's modifications implemented ,the codes give mass fractions that are in close agreement with each other for the case of $Y_{\min} = 0.0$.

tions stay in close agreement for non-zero $Y_{\min}$, as shown in Table (2.9) for $Y_{\min} = 10^{-25}$. The values of $X_{^4He}$ change from their $Y_{\min} = 0.0$ values by less than 0.0001, and they still agree with each other to within 0.0001. Figures (2.15) show that the codes have this agreement regardless of the value of η_{10}.

With the convergence order and effect of $Y_{\min}$ brought in agreement between the codes one can compare the effects of the differences in equations between the codes. The Thomas et al code's expression for $d\rho_e/dT$

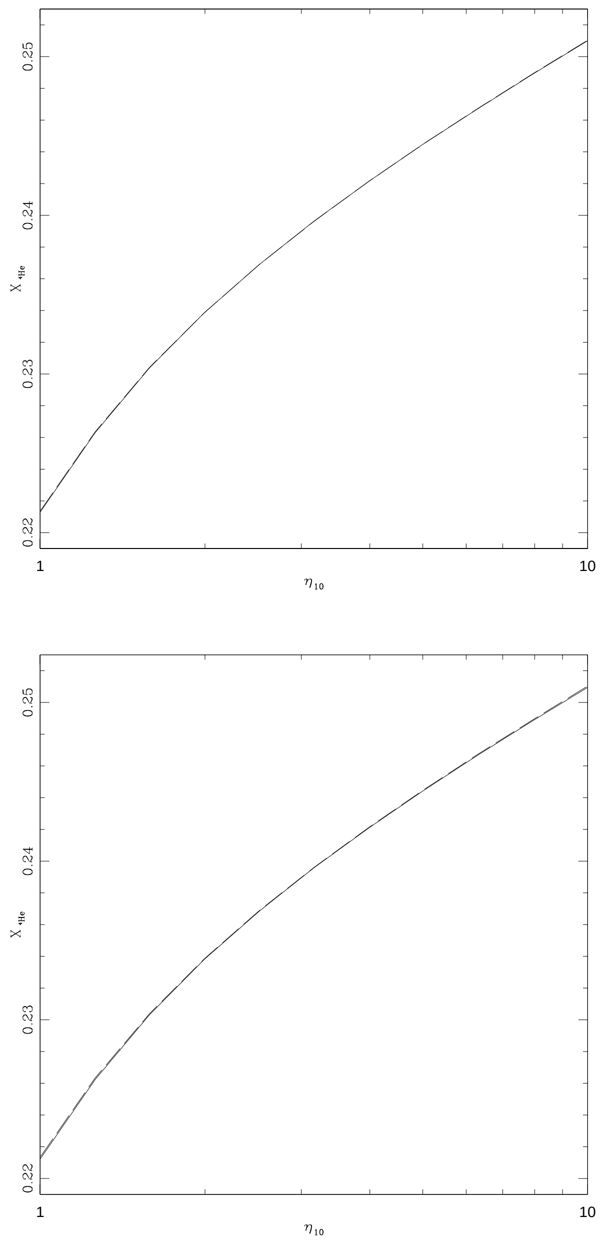

Figure 2.15: $X_{^4\mathrm{He}}$ as a function of η_{10} for the cases of $Y_{\mathrm{min}} = 0.0$ and $Y_{\mathrm{min}} = 10^{-25}$. $X_{^4\mathrm{He}}$ for both codes are graphed, but the differences are imperceptible at this scale.

$$\frac{d\rho_{\mathrm{e}}}{dT} = \frac{\partial\rho_{\mathrm{e}}}{\partial T} + \frac{\partial\rho_{\mathrm{e}}}{\partial\phi_{\mathrm{e}}}\frac{\partial\phi_{\mathrm{e}}}{\partial T}$$

has the term that accounts for ϕ_{e}'s temperature dependence that the Texas code does not have. But actually the $(\partial\rho_{\mathrm{e}}/\partial\phi_{\mathrm{e}})(\partial\phi_{\mathrm{e}}/\partial T)$ term is as much as 17 orders of magnitude smaller than the $(\partial\rho_{\mathrm{e}}/\partial T)$ term. These two terms don't come to the same order of magnitude until when $T =$ around 0.2 GK, long after most abundances have reached their final values and when ρ_{e} is too small to be significant. Both h_v and T are time dependent in the Thomas et al code's equation for $\rho_b = h_v(15a/\pi^2)T^3$. But dh_v/dt is derived from the equation $h_v = \mathrm{const}/(RT)^3$. From that equation one can derive the Texas code's Equation (2.2), $\rho_b R^3 = \mathrm{const}$, as well. ϕ_{e} plays a significant part in the Thomas et al code's run only in the initialization of ρ_b. Figure (2.16) shows graphs of ρ_{e}, p_{e}, ρ_ν, ρ_b, $\lambda(\mathrm{n}\to\mathrm{p})$ and $\lambda(\mathrm{p}\to\mathrm{n})$ as functions of temperature. The graphs are actually for both codes, but they coincide to the point that one can't tell them apart in Figure (2.16).

This author does convergence tests for both codes in their final forms and get the equations

$$X_{^4\mathrm{He}} = 0.2391419133 - (0.1204714449 \times 10^{-3})d^2$$

for the Texas code and

$$X_{^4\mathrm{He}} = 0.2390662112 - (0.3263425056 \times 10^{-4})d^2$$

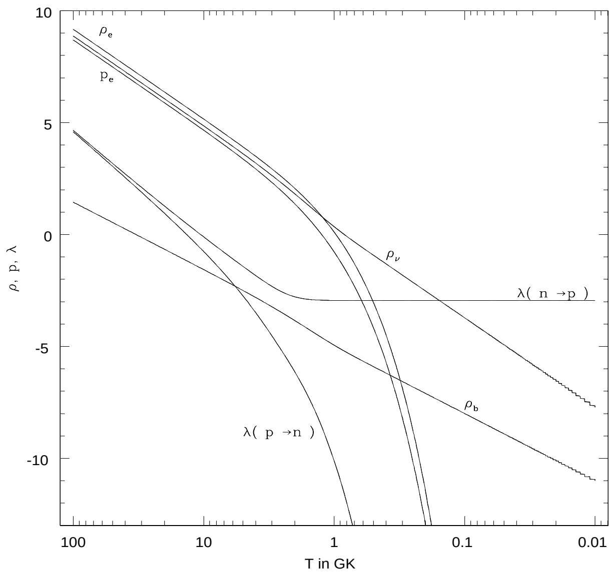

Figure 2.16: Quantities such as the energy densities ρ_γ, ρ_e, ρ_ν, the pressure p_e, and the neutron/proton conversion rates have nearly identical graphs in both codes.

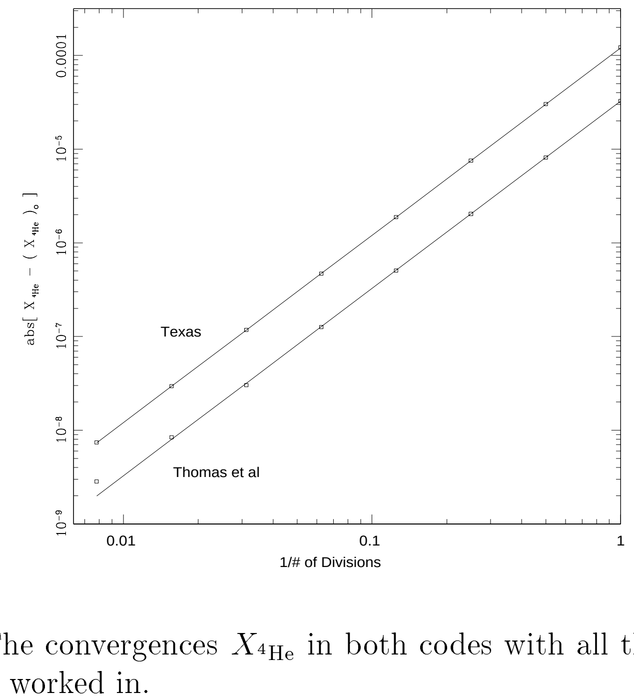

Figure 2.17: The convergences $X_{^4\mathrm{He}}$ in both codes with all the modifications of this chapter worked in.

isotope	Thomas et al X	Texas X
n	$0.536042514 \times 10^{-15}$	$0.5183261081 \times 10^{-15}$
p	0.7608156967	0.7608642342
d	$0.1211664296 \times 10^{-3}$	$0.1220484312 \times 10^{-3}$
^{3}H	$0.585553688 \times 10^{-6}$	$0.589702407 \times 10^{-6}$
^{3}He	$0.3611405145 \times 10^{-4}$	$0.3622248496 \times 10^{-4}$
^{4}He	0.2390194809	0.2389701702
^{6}Li	$0.1447297749 \times 10^{-12}$	$0.1457090806 \times 10^{-12}$
^{7}Li	$0.3414171454 \times 10^{-9}$	$0.3435117277 \times 10^{-9}$
^{7}Be	$0.2827907528 \times 10^{-9}$	$0.2784141878 \times 10^{-9}$
^{9}Be	$0.1071697077 \times 10^{-16}$	$0.1086466968 \times 10^{-16}$
^{10}B	$0.9293751658 \times 10^{-18}$	$0.9379254692 \times 10^{-18}$
^{11}B	$0.998592013 \times 10^{-16}$	$0.9677258428 \times 10^{-16}$
^{12}C	$0.3017256027 \times 10^{-13}$	$0.2994422594 \times 10^{-13}$
^{13}C	$0.2061400405 \times 10^{-14}$	$0.2033703883 \times 10^{-14}$
^{14}C	$0.6492052092 \times 10^{-13}$	$0.6468017788 \times 10^{-13}$
^{14}N	$0.1317883048 \times 10^{-12}$	$0.1313246722 \times 10^{-12}$
^{16}O	$0.7620063819 \times 10^{-17}$	$0.754877117 \times 10^{-17}$
^{19}F	$0.1618658555 \times 10^{-20}$	$0.1621937231 \times 10^{-20}$
^{20}F	$0.2432620156 \times 10^{-20}$	$0.2437402872 \times 10^{-20}$
^{21}Ne	$0.1938954314 \times 10^{-20}$	$0.1942391743 \times 10^{-20}$

Table 2.9: The codes' results remain in close agreement for the case of $Y_{\min} = 0.0$.

for the Thomas et al code. Figure (2.17) graphs the actual data and these best fit lines. The line for the Thomas et al code has a good fit, but the data starts diverging from the line for the most divisions, when the difference between $X_{^4\mathrm{He}}$'s actual value and the convergent value is eight orders of magnitude smaller than $X_{^4\mathrm{He}}$ itself. The Texas code's $X_{^4\mathrm{He}}$ converges to nearly the same value as in Figure (2.5), while the Thomas et at code converges to a slightly higher value. The difference in convergent values is where the differences between the codes have their ultimate effect, but this difference is still less than 0.0001.

2.5 The Isotope Network

Figures (2.18) to (2.30) show the most important reactions for a handful of isotopes heavier than ^{7}Be. It turns out that reactions that produce these heavier isotopes don't change the abundances of ^{7}Be and lighter isotopes significantly. But in the process of determining that this author mapped out a detailed description of the production of the more important of the heavier isotopes. A specific reaction will change the abundance of an isotope i by an amount $\Delta Y(i)$ at each timestep. These figures graph $\Delta Y(i)$ for each different reaction, the graphs corresponding to the reaction's contribution to the right-hand side of Equation (2.19) times Δt. Reactions that create a particular isotope are graphed with solid lines while reactions that destroy the isotope are graphed with dashed lines.

2.5.1 ^{9}Be, ^{10}B, ^{11}B

Figures (2.18) show the changes in $Y(^9\text{Be})$ due to reactions that create ^{9}Be or destroy ^{9}Be. Production of ^{9}Be comes primarily from ^{7}Li and ^{8}Li through the reactions p + ^{8}Li $\rightarrow^9$Be and t + ^{7}Li $\rightarrow$ n + ^{9}Be. But at temperature T = 0.75 GK when the reaction rates peak the abundance $Y(^9\text{Be})$ has an order of magnitude of 10^{-15}, the same order of magnitude as produced by reactions such as d + ^{8}Li $\rightarrow$ n + ^{9}Be or p + ^{9}Li $\rightarrow$ n + ^{9}Be. Figure (2.18b) shows that ^{9}Be is primarily converted to ^{4}He and ^{6}Li. The reaction ^{9}Be $\rightarrow$ n + 2 (^{4}He) is actually an endoergic reaction. But during nucleosynthesis ^{9}Be is apparently fragile enough that most nuclei are disassociated by photons into neutrons and ^{4}He nuclei.

Figure (2.19) shows the most significant reactions that create and de-

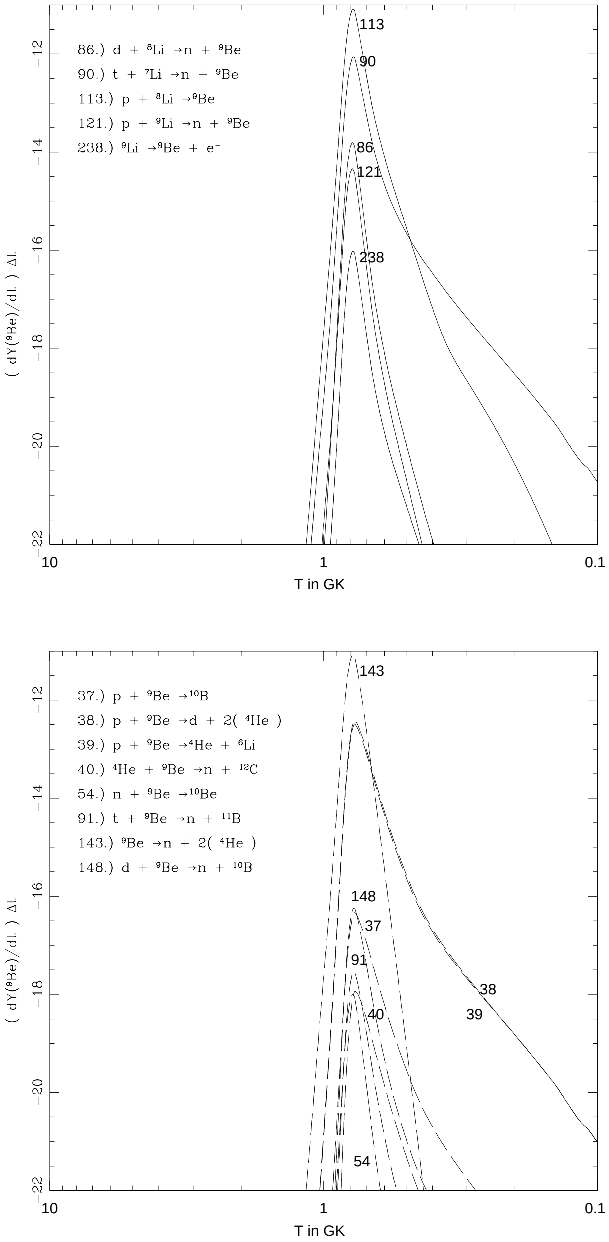

Figure 2.18: The most significant reactions that create or destroy ^{9}Be.

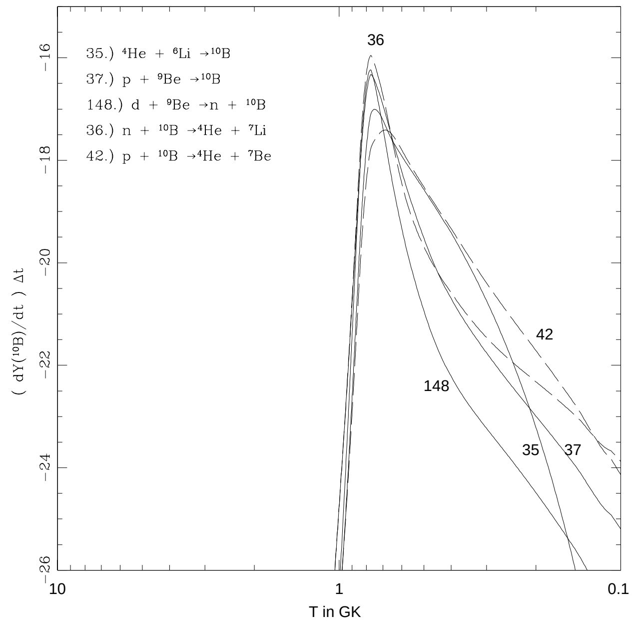

Figure 2.19: The most significant reactions that create or destroy ^{10}B.

stroy ^{10}B. Fewer reactions have a substantial effect on ^{10}B than for ^{9}Be. ^{10}B production comes primarily from ^{9}Be through the reactions p + ^{9}Be $\rightarrow^{10}$B and d + ^{9}Be $\rightarrow$ n + ^{10}B. The changes $\Delta Y(^{10}\mathrm{B})$ due to these reactions never reach more than an order of 10^{-16} because of the small abundance of ^{9}Be. $Y(^{10}\mathrm{B})$ itself never has a magnitude higher than 10^{-18}. After nucleosynthesis the reaction ^{4}He + ^{6}Li $\rightarrow^{10}$B becomes the most significant reaction that produces ^{10}B. The rate for the reaction p + ^{10}Be $\rightarrow^{4}$He + ^{7}Be becomes slightly larger than the rate for ^{4}He + ^{6}Li $\rightarrow^{10}$B, and the reactions have an overall effect of converting ^{10}B to ^{7}Be. $Y(^{10}\mathrm{B})$ decreases after nucleosynthesis until $T = 0.2$ GK when the abundance reaches a final order of 10^{-19}.

Figures (2.20) show the reactions that create and destroy ^{11}B respectively. ^{11}B production comes primarily from ^{7}Li via the reaction ^{4}He + ^{7}Li

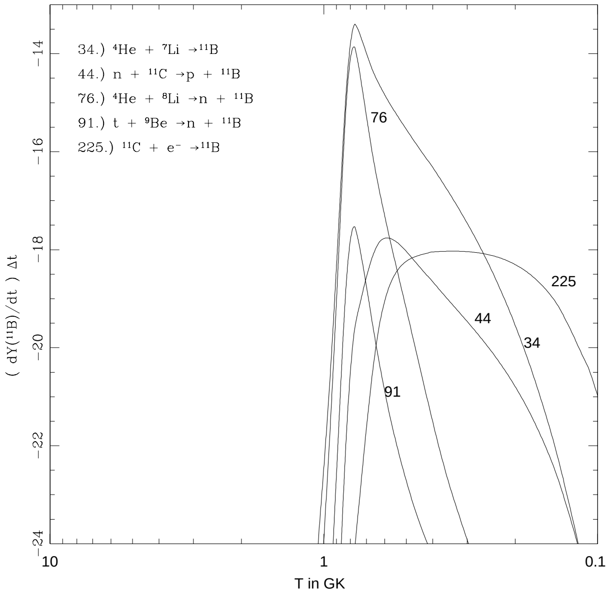

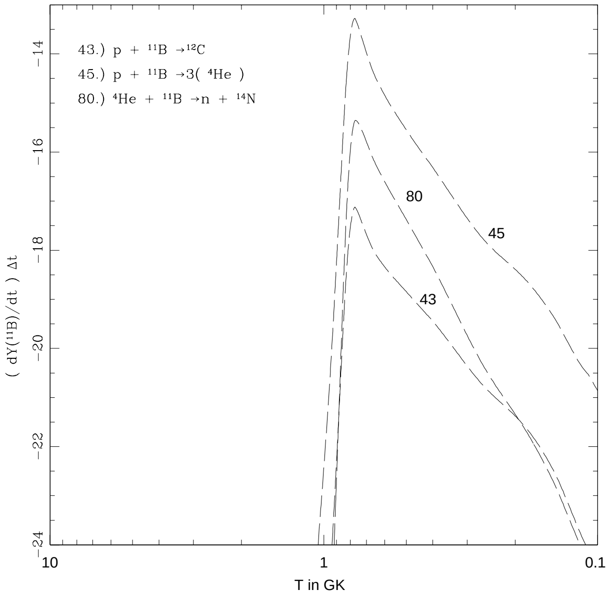

Figure 2.20: The most significant reactions that create or destroy ^{11}B.

$\rightarrow {}^{11}$B, and from ^{8}Li by the reaction ^{4}He + ^{8}Li $\rightarrow$ n + ^{11}B (^{8}Li itself is produced from ^{7}Li through the reaction n + ^{7}Li $\rightarrow {}^{8}$Li.). The reaction p + ^{11}B $\rightarrow$ 3(^{4}He) then converts ^{11}B mostly to ^{4}He. At temperature T = around 0.25 GK the decay of ^{11}C to ^{11}B becomes the most significant producer of ^{11}B. The abundance $Y({}^{11}\text{B})$ increases again, briefly until it reaches a final value. Figure (2.21) shows that the reaction ^{4}He + ^{7}Be $\rightarrow {}^{11}$C produces most of ^{11}C. During nucleosynthesis the abundance $Y({}^{11}\text{C})$ exceeds $Y({}^{11}\text{B})$. But ^{11}C beta decay eventually converts all ^{11}C to ^{11}B.

All three isotopes, ^{9}Be, ^{10}B, and ^{11}B, have destruction reactions that balance out creation reactions during nucleosynthesis. The abundances of these three isotopes peak during nucleosynthesis and then fall to values too small to observe. These isotopes are overwhelmingly converted to lighter isotopes such as ^{4}He and ^{6}Li.

2.5.2 The Six-Isotope Cycle between Carbon and Nitrogen

The reaction ^{4}He + ^{11}B $\rightarrow$ n + ^{14}N is not as significant to ^{11}B as the reaction p + ^{11}B $\rightarrow$ 3(^{4}He) is. But Figure (2.22) shows that this reaction is the main reaction for production of ^{14}N. The reaction n + ^{14}N $\rightarrow$ p + ^{14}C is the main reaction for ^{14}N destruction. During nucleosynthesis the rate for ^{4}He + ^{11}B $\rightarrow$ n + ^{14}N is larger than the rate for n + ^{14}N $\rightarrow$ p + ^{14}C, and for T between 0.9 GK and 0.4 GK that creation reaction rate is considerably larger than the destruction reaction rates, as shown in Figure (2.22). $Y({}^{14}\text{N})$ can reach an order of magnitude of 10^{-14}, and flattens out to a final value rather than decreasing first like ^{9}Be, ^{10}B and ^{11}B.

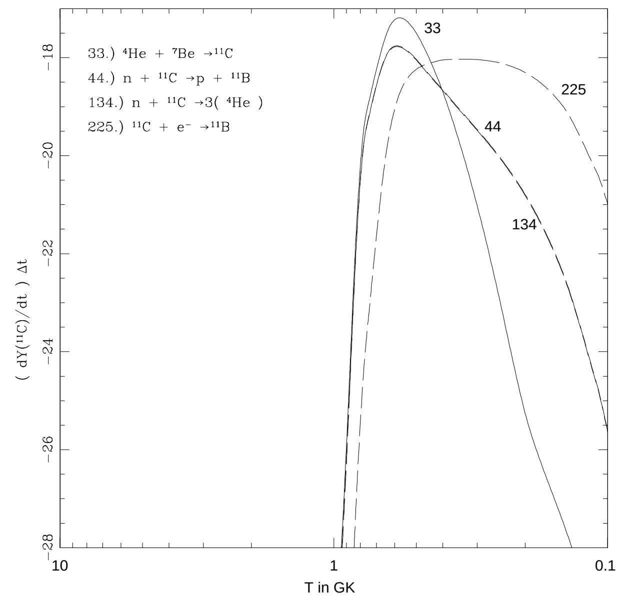

Figure 2.21: The most significant reactions that create or destroy ^{11}C.

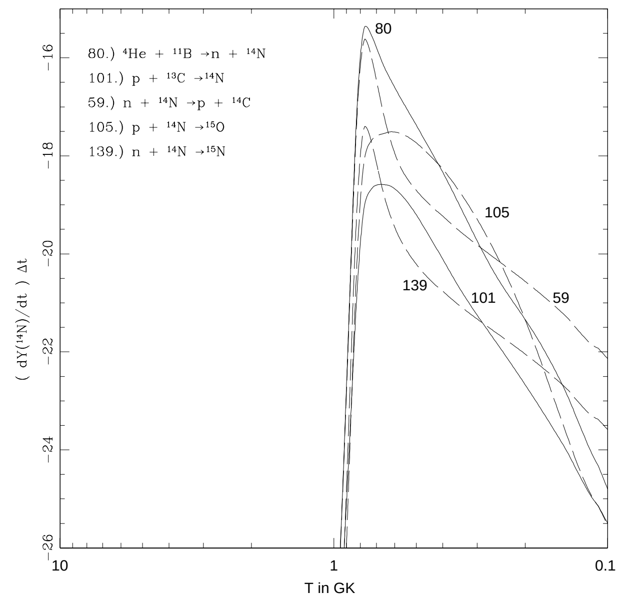

Figure 2.22: The most significant reactions that create or destroy ^{14}N.

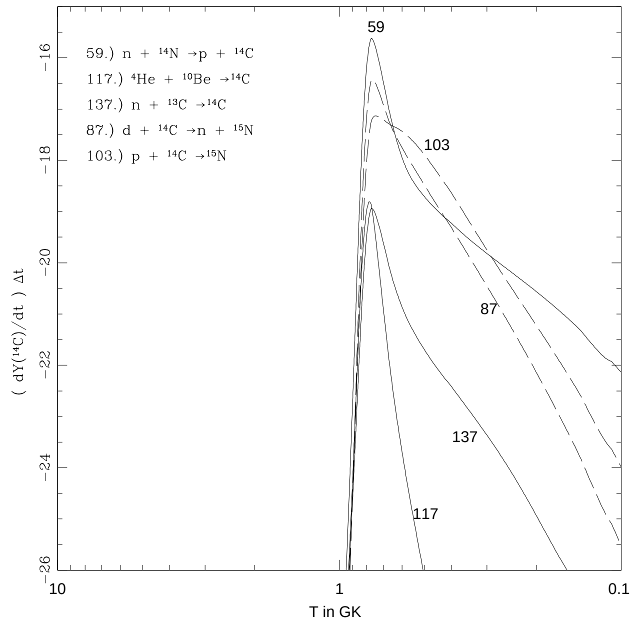

Figure 2.23: The most significant reactions that create or destroy ^{14}C.

Figure (2.23) shows that the primary destruction reaction of ^{14}N is the primary production reaction of ^{14}C. ^{14}C in turn is converted to ^{15}N via the reactions d + ^{14}C $\rightarrow$ n + ^{15}N and p + ^{14}C $\rightarrow^{15}$N. Like with ^{14}N, production of ^{14}C is more than destruction of ^{14}N during nucleosynthesis. $Y(^{14}\mathrm{C})$ asymptotes to a value of over 10^{-15}. The destruction reaction rates of ^{14}C overtake ^{14}C's creation reaction rates more quickly than the destruction reaction rates of ^{14}N overtake the ^{14}N's creation reaction rates. The graph for $Y(^{14}\mathrm{C})$, unlike for $Y(^{14}\mathrm{N})$, has a slight dip as a result.

Figure (2.24) shows that those two reactions that convert ^{14}C to ^{15}N are the most significant reactions that produce ^{15}N during nucleosynthesis. After nucleosynthesis, two reactions that produce ^{15}N from ^{15}O become significant as well. ^{15}N has only one significant destruction reaction, p + ^{15}N $\rightarrow^{4}$He +

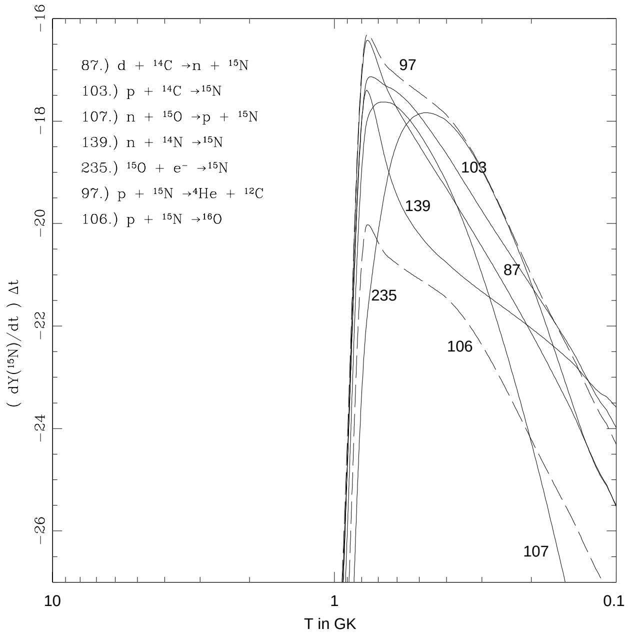

Figure 2.24: The most significant reactions that create or destroy ^{15}N.

^{12}C. The rate of this reaction is larger than the creation reaction rates during nucleosynthesis. The abundance $Y(^{15}\mathrm{N})$ peaks at just above 10^{-17} at $T =$ 0.74 GK and then decreases. At $T = 0.54$ GK, production of ^{15}N via electron capture of ^{15}O starts to dominate among the creation reactions. The creation reaction rates added up become larger than the destruction rate from p + ^{15}N $\rightarrow ^4$He + ^{12}C, and $Y(^{15}\mathrm{N})$ increases again until it asymptotes to a final value of around 3 $\times 10^{-18}$.

p + ^{15}N $\rightarrow ^4$He + ^{12}C is the primary reaction that produces ^{12}C. Figure (2.25) shows this reaction along with reactions that create ^{12}C from ^{9}Be, ^{11}B and ^{12}B. Those reactions are of secondary importance to the abundances of ^{9}Be and ^{11}B, and their rates are an order of magnitude smaller than the rate for p + ^{15}N $\rightarrow ^4$He + ^{12}C during nucleosynthesis. Even smaller is the rate for

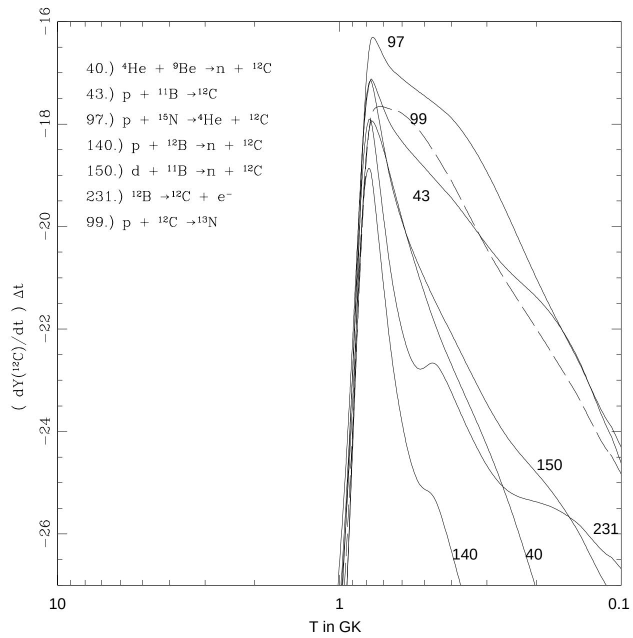

Figure 2.25: The most significant reactions that create or destroy ^{12}C.

the only significant reaction that destroys ^{12}C, p + ^{12}C $\rightarrow^{13}$N. $Y(^{12}\mathrm{C})$ can asymptote to a value of nearly 3.0 $\times 10^{-15}$. The flow of nucleons that reach the heavier isotopes instead of getting incorporated into ^{4}He mostly end up getting incorporated into ^{12}C.

The relatively small destruction reaction of ^{12}C mentioned above is the primary production reaction of ^{13}N. Figure (2.26) shows p + ^{12}C $\rightarrow^{13}$N, and the most significant destruction reactions of ^{13}N, n + ^{13}N $\rightarrow$ p + ^{13}C and e$^-$+^{13}N $\rightarrow^{13}$C. The rate for n + ^{13}N $\rightarrow$ p + ^{13}C is nearly equal to the rate for p + ^{12}C $\rightarrow^{13}$N during and after nucleosynthesis, and electron capture of ^{13}N dominates after nucleosynthesis. As a result nearly all ^{13}N is converted to ^{13}C.

Figure (2.27) shows that n + ^{13}N $\rightarrow$ p + ^{13}C and e$^-$+^{13}N $\rightarrow^{13}$C are the primary creation reactions of ^{13}C, and that p + ^{13}C $\rightarrow$ ^{14}N is the most

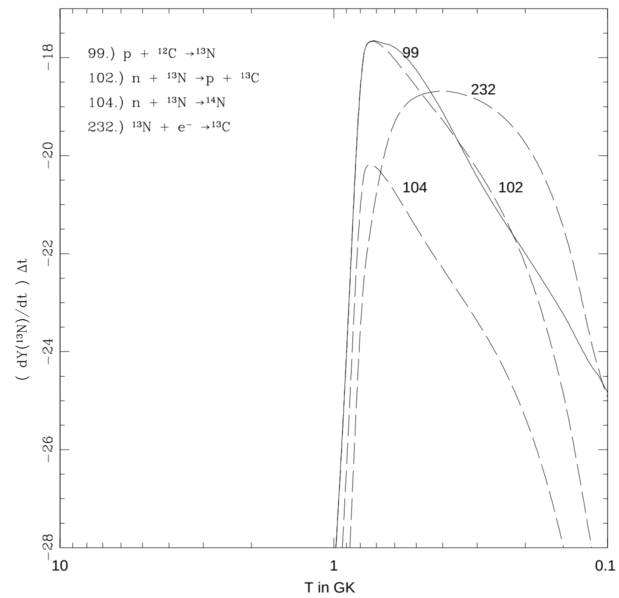

Figure 2.26: The most significant reactions that create or destroy ^{13}N.

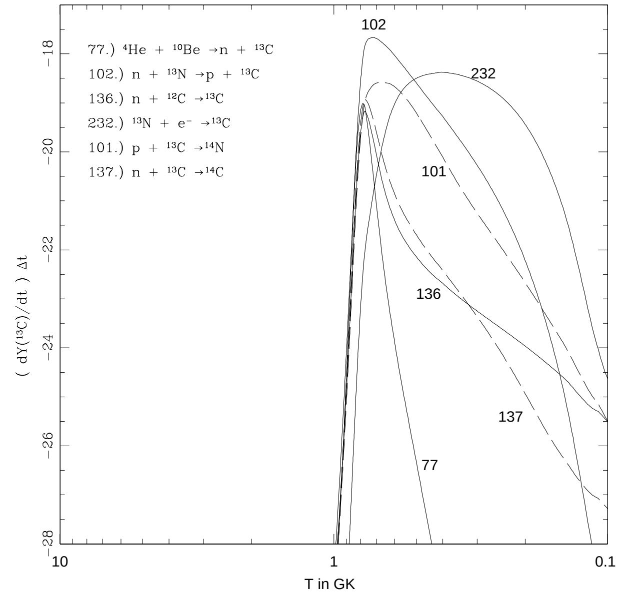

Figure 2.27: The most significant reactions that create or destroy ^{13}C.

significant destruction reaction. p + ^{13}C $\rightarrow$ ^{14}N has a smaller rate than the two creation reaction rates. The abundance $Y(^{13}\mathrm{C})$ asymptotes to a final value of just over 10^{-16}.

The reaction p + ^{13}C $\rightarrow$ ^{14}N brings the nucleon flow back to ^{14}N. So from ^{11}B the nucleon enters through ^{14}N a cycle between the isotopes ^{14}C, ^{15}N, ^{12}C, ^{13}N, ^{13}C, and back to ^{14}N. Most nucleons in the flow end up as part of ^{12}C nuclei, or ^{14}N or ^{14}C.

2.5.3 ^{16}O

^{16}O is produced primarily from ^{15}N. But ^{16}O is also produced through a channel that goes from ^{14}C to ^{15}C to ^{16}N.

n + ^{14}C $\rightarrow$^{15}C is the only reaction that creates significant amounts of ^{15}C. With a rate five orders of magnitude smaller than the rates of the most significant reactions that destroy ^{14}C, this reaction has no influence on the final value of ^{14}C's abundance. In the temperature range where the destruction reactions of ^{14}C dominate ^{14}C depletion is enough to make n + ^{14}C $\rightarrow$^{15}C start increasing again after peaking, reaching a second peak when the directions of the reaction fall out of equilibrium with each other. Figure (2.28) shows this reaction, as well as the four significant reactions that destroy ^{15}C. These graphs mimic the shape of the graph for n + ^{14}C $\rightarrow$^{15}C. Ultimately, ^{15}C decay into ^{15}N matches the rate of n + ^{14}C $\rightarrow$^{15}C, depleting ^{15}C.

Figure (2.29) shows that the reaction p + ^{15}C $\rightarrow$^{16}N is the primary creation reaction of ^{16}N for temperatures around T = 0.5 GK, while n + ^{15}N $\rightarrow$^{16}N is the main creation reaction for temperatures around 0.8 GK, near the onset of nucleosynthesis. The rates of the destruction reactions p + ^{16}N

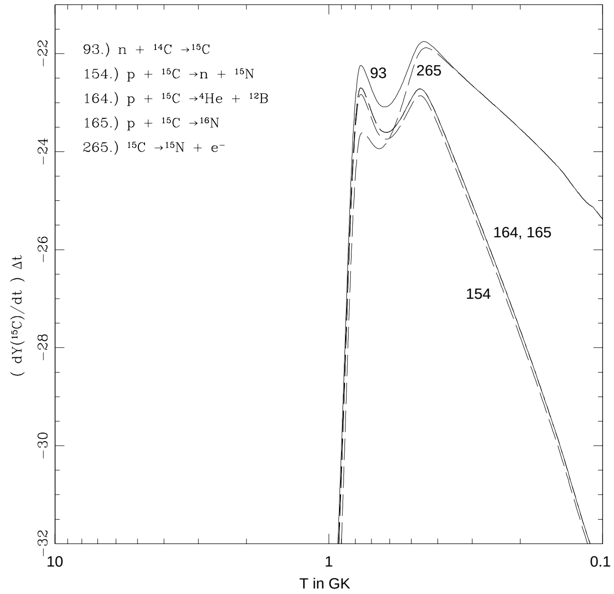

Figure 2.28: The most significant reactions that create or destroy ^{15}C.

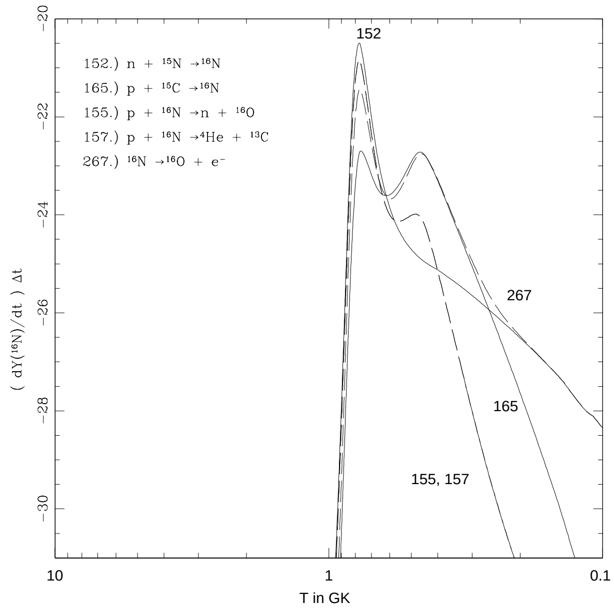

Figure 2.29: The most significant reactions that create or destroy ^{16}N.

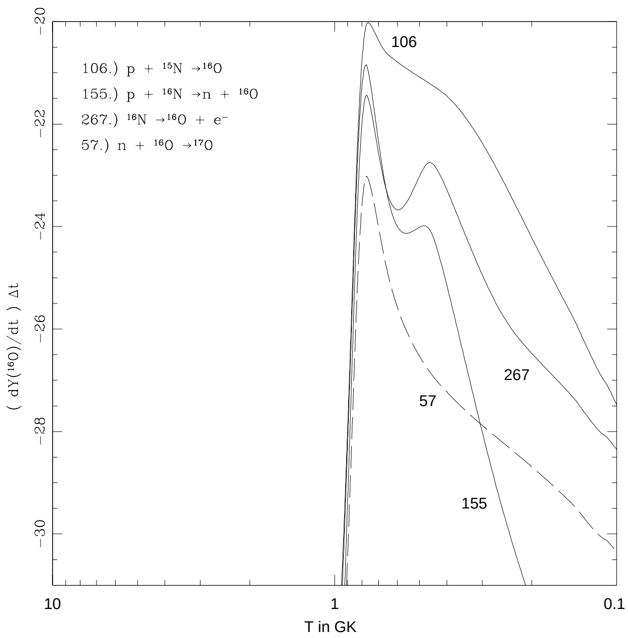

Figure 2.30: The most significant reactions that create or destroy ^{16}O.

→ n + ^{16}O and ^{16} N →^{16}O + e^{-} nearly match the creation reaction rates, ultimately converting most ^{16}N to ^{16}O. Figure (2.30) shows those two reactions as significant creation reactions of ^{16}O, but neither reaction rate is as large as the rate for p + ^{15}N →^{16}O. ^{16}O then comes primarily from ^{15}N, though ^{15}N is not considerably depleted by this channel. ^{16}O also has only one important destruction reaction, n + ^{16}O →^{17}O, and that is considerably smaller than the creation reactions. So $Y(^{16}\text{O})$ asymptotes to a value of 4 $\times 10^{-19}$.